Magnitude of large-transverse-momentum cross sections

R. Blankenbecler and S. J. Brodsky
Stanford Linear Accelerator Center, Stanford University, Stanford, California 94305

J. F. Gunion
Department of Physics, University of California, Davis, California 95616
(Received 5 December 1977)

Consistent values for the fundamental dimensional coupling constants of hadrons to their valence quarks are determined from large-momentum-transfer elastic scattering, photoproduction, form factors, and momentum distributions. We then show that the constituent-interchange-model hard-scattering subprocesses $Mq \to Mq$ and $Bq \to Bq$ (and their crossing variants) are of sufficient magnitude to account for the normalization as well as the kinematic behavior in p_T, angle, and s of single-particle large-transverse-momentum inclusive cross sections. The crossover point where p_T^{-4} scale-invariant $qq \to qq$ and gluon terms may dominate the cross section is computed. Jet cross sections and charge correlations are also discussed. We also give analytic formulas for inclusive cross sections in general hard-scattering models. Spectator and dimensional-counting rules are given which determine the scaling behavior in p_T, $\epsilon = \mathfrak{M}^2/s$, and $\theta_{\text{c.m.}}$.

I. INTRODUCTION

In the last few years the phenomena of high-transverse-momentum physics have become an important tool in unraveling the internal structure and basic interaction mechanisms of hadrons. At the quark level, two competing mechanisms have been intensively studied: quark-quark scattering and constituent-interchange mechanisms involving quark-hadron vertices only, such as $qM \to qM$. Both mechanisms are capable of producing particles at high transverse momentum. The 90° inclusive cross sections are predicted to be of the form ($\epsilon \equiv \mathfrak{M}^2/s = 1 - x_T$)

$$E\frac{d\sigma}{d^3p} \propto \begin{cases} p_T^{-4}\epsilon^{F}, & qq \to qq \\ p_T^{-8}\epsilon^{F'}, & qM \to qM \\ & q\bar{q} \to MM \\ p_T^{-12}\epsilon^{F''}, & qB \to qB \\ & q\bar{q} \to B\bar{B} \end{cases}$$

if one assumes an underlying scale-invariant theory. For p_T smaller than 8 GeV/c, the Fermilab[1,2] and CERN ISR[3,4] data indicate that the p_T^{-4} behavior is not present, whereas, the p_T^{-8} behavior and values of F' predicted by the constituent-interchange model (CIM) appear to describe the cross sections for meson production. (For example, the quoted fit to the Chicago-Princeton data[1] for $pp \to \pi + X$ at $\theta_{\text{c.m.}} = 90°$ gives $p_T^{-8.2}\epsilon^{9.0}$; the CIM prediction is $p_T^{-8}\epsilon^{9}$ from quark-meson scattering.) The first discussions of inclusive production of mesons at large transverse momentum were given by Berman and Jacob, and Berman, Bjorken, and Kogut,[5] who argued that scaling in electromagnetic processes must lead eventually to scale-invariant p_T^{-4} behavior at fixed x_T. The CIM,[6,7] on the other hand, was developed in order to explain exclusive scattering at low energies. When applied to inclusive scattering, it predicts that the numerically dominant terms from quark-meson scattering should behave as p_T^{-8}. This result was based on a fundamental scale-invariant quark-quark interaction which will eventually produce a p_T^{-4} behavior unless it is very strongly suppressed. In this paper, we shall reconcile these mechanisms by studying the relative normalizations of CIM diagrams and the quark-quark-gluon contributions.

The absence of p_T^{-4} terms in the meson yields has led quark-scattering advocates to consider two modifications to the scale-invariant $qq \to qq$ cross section, chosen so as to yield approximate $1/p_T^8$ behavior. One approach is to assume scale breaking in the structure functions and the quark-quark amplitude.[8] Alternatively, scaling can be preserved in the distribution functions, and the quark-quark cross section can be chosen to fit the data [in the manner of Field and Feynman (FF)].[9] These approaches share several difficulties:

(a) Elastic fixed-angle cross sections at large p_T cannot be described using the same basic $qq \to qq$ subprocess employed for inclusive predictions (see Ref. 7 for details).

(b) In quantum chromodynamics (QCD) models the standard value for the gluon coupling constant ($\alpha_s \sim 0.3$) gives a cross section an order of magnitude below the data for $p_T \lesssim 5$ GeV. In the FF model the quark-quark cross section is fitted to the form $d\sigma/dt(qq \to qq) = C/st^3$, where $C \simeq 6 \times 10^3$ GeV^4 which seems uncomfortably large. We note that the form $1/st^3$ or $1/su^3$ is exactly that predicted for the $qM \to qM$ subprocess, and is in fact characteristic of spin-$\frac{1}{2}$ exchange, not vector exchange.

(c) In the FF model the p_T^{-12} behavior for proton production[1] is not accounted for. One can appeal to "leading-particle" effects, but then one is somewhat embarrassed by having to omit them in estimating meson yields from pion beams.

(d) In models with quark (or gluon) fragmentation into the observed hadron, the away-side jet is forced to carry transverse momentum of order 20% in excess of the trigger p_T. Reconciling this with experiment may require very large transverse-momentum fluctuations in the hadronic wave functions.

(e) Models based on quark-quark scattering generally predict no correlations between the charge of the trigger particle and the charge of particles in the away-side jet. However, striking correlations for high p_T K^- and $\bar{p}$ triggers have been observed by the British-French-Scandinavian (BFS) group at the ISR.[10] We also note that there is no theoretical justification of employing a factorized form for scale violations in the asymptotic-freedom-type model, and the actual predictions for a model such as QCD are not known unambiguously.

In principle there could be scale-breaking corrections of the asymptotic-freedom type to the dimensional-counting rules and the CIM forms for the quark-hadron amplitudes. However, the basic scaling prediction for the proton form factor $t^2F_p(t) \to$ const appears to hold within ~5% accuracy for $4 < |t| < 36$ GeV^2, suggesting that amplitudes involving color-singlet hadron vertices may not have strong QCD corrections.[11] Consequently *our analysis here will be restricted to a strictly scale-free theory*.

As we shall review here, the dynamical forms and the quark counting predictions based on CIM subprocesses are in good agreement with experiment for all produced particle types. The uncertainty in the CIM approach has always been in the absolute magnitude of the various contributions. We will show that the normalization of the experimental inclusive cross sections is in reasonable agreement with theoretical expectations based on form factors, structure functions, and 90° elastic scattering measurements at low energies. We shall predict which subprocesses should dominate production of a given particle in a given kinematical regime. Our normalizations will be seen to be inherently uncertain by factors of 2 or 3; however, predictions for certain cross-section ratios have much less uncertainty.

In a purely scale-invariant theory, the dominance of the CIM diagrams over $qq \to qq$ contributions in the thoroughly explored experimental regime $p_T < 8$ GeV/c is in fact expected if the conventional value of $\alpha_s \lesssim 0.3$ is used (see Sec. IX). In part, this is because the trigger hadron can be formed directly in the hard-scattering CIM subprocess. Quark-quark and gluon scattering is predicted to become dominant for $p_T \gtrsim 8$–10 GeV/c and will be an important contribution to jet-trigger experiments at much lower values of p_T.

Briefly, the organization of the paper will be as follows:

In Sec. II, a short summary and catalog of experimental results for elastic and inelastic high-transverse-momentum cross sections and a discussion of trigger bias will be given. In Sec. III, we present a review of structure functions and related sum rules, general formulas for elastic and inclusive cross sections, and the various contributing CIM subprocess forms. Also, coupling constants are precisely defined. Section IV presents the determination of certain important coupling constants from elastic scattering measurements. In Sec. V, the determination of the above coupling constants from the behavior of structure functions is made and their consistency with the results of Sec. IV is noted. In Sec. VI, inclusive cross sections for *proton beams* are described in detail for many different particle yields. *Antiproton beams* are briefly discussed. Section VII presents a discussion on inclusive cross sections for a *pion beam*. In Sec. VIII, the inclusive-exclusive connection is examined. In Sec. IX, inclusive cross sections based on *quark-quark scattering* are computed. We discuss jet-jet cross sections in Sec. X, and in Sec. XI and XII a general discussion, a few remarks, and some conclusions are given.

A check of our analytical approximation is made in Appendix A. A detailed discussion of the definition of the quark-hadron coupling constants and their determination from the asymptotic behavior of the meson and nucleon form factors is given in Appendix B.

II. CATALOG OF EXPERIMENTAL RESULTS

We will parametrize fixed-angle (90° center of mass) exclusive two-body cross sections at large s in the form

$$\left.\frac{d\sigma}{dt}\right|_{90^\circ} = Es^{-n}. \tag{2.1}$$

A review of the relevant data is given in Ref. 7. We employ throughout this paper pure GeV units. Inclusive large-p_T cross sections at 90° center of mass from Fermilab[1,2] and the ISR[3,4] can be fitted to the form ($\epsilon = 1 - 2p_T/\sqrt{s} = 1 - x_T$)

$$E\left.\frac{d\sigma}{d^3p}\right|_{90^\circ} = I\epsilon^F(p_T^2)^{-N}, \quad \begin{cases} x_T > 0.2, \\ 2 < p_T < 8 \text{ GeV}/c \end{cases} \tag{2.2}$$

Table I summarizes the values for I, N, F, and E, n for the various well-known cross sections of in-

TABLE I. Parameters for cross sections [see Eqs. (2.1) and (2.2)] in pure GeV units.

Reaction	E	n	
$pp \to pp$	1.2×10^9	10	
$\pi^\pm p \to \pi^\pm p$	2.0×10^5	8	
$\pi^- p \to \pi^0 n$	2.5×10^4	8	
$\gamma p \to \pi^+ n$	2.6×10^1	7	
Reaction	I	N	F
$pp \to \pi^{+,0,-} X$	(9, 8, 7)	4	9
$pp \to K^+ X$	5	4	9
$pp \to pX$	500	6	7
$\pi^\pm p \to \pi^0 X$	3.5	4	7

terest. For N and F we have chosen the nearest *integer* values, and then fitted the normalization constant I. The reactions $pp \to K^- X$ or $\bar{p}X$ near 90° are characterized by the following behavior:

$$\frac{E\frac{d\sigma}{d^3p}(pp \to K^- X)}{E\frac{d\sigma}{d^3p}(pp \to K^+ X)} \approx 1.0\epsilon^{3.5}, \tag{2.3}$$

$$\frac{E\frac{d\sigma}{d^3p}(pp \to \bar{p}X)}{E\frac{d\sigma}{d^3p}(pp \to pX)} \approx 0.3\epsilon^{6.9\pm2.4}(p_T{}^2)^{1.4\pm1.3}. \tag{2.4}$$

The γ/π^0 ratio in pp collisions is reported to be as high as 30%.[12] The $\pi^\pm p \to \pi^0$ form quoted in Table I uses the measured ratio $\pi^+ p \to \pi^0/pp \to \pi^0$ from Donaldson *et al.*[2]

In the case of the inclusive cross section, it is important to establish the percentage of trigger particles which are "prompt," as opposed to those which arise indirectly from a decaying high-p_T resonance or virtual state. This percentage is roughly determined phenomenologically by examining the x_E distribution

$$x_E = \frac{(p_T)_{\text{opposite}}}{(p_T)_{\text{trigger}}}, \tag{2.5}$$

where x_E measures the distribution in transverse momentum of a hadron produced in the hemisphere opposite the trigger pion. If the trigger π is "prompt" then the maximum value of x_E is 1, whereas when it is the product of a resonance (or fragmentation process) then $(x_E)_{\max} > 1$–the parent system (and hence the balancing away-side system) must carry more p_T than the trigger pion. The data[13] appear consistent with a mean value

$$\langle (x_E)^{\max} \rangle \sim 1.1 .$$

Using

$$(x_E)^{\max} \sim \begin{cases} 1 \text{ prompt}, \\ 1.1 \text{ two-body resonance}, \\ 1.2 \text{ three-body resonance} \end{cases}$$

(calculated using the local-exponent approach of Ellis *et al.*),[14] we obtain conditions for the fraction of events that are prompt, two-, and three-body resonances:

$$f_p + f_2 + f_3 = 1$$

and

$$f_p + 1.1 f_2 + 1.2 f_3 = 1.1 .$$

Assuming that $f_2 \sim f_3$, we estimate for pions

$$f_p \sim \tfrac{1}{3} . \tag{2.6}$$

Allowing for transverse-momentum fluctuations of the initial participants in the high-p_T subprocesses results in a slight decrease in f_p. This type of ratio (which is important for the estimate of jet cross sections as discussed in Sec. XI) is expected theoretically if prompt spin-1 mesons ($\rho, K^*, \ldots$) are produced (with the statistical weight) three times as frequently as prompt pions. This yield is consistent with the experimental ratio[15a]

$$\rho/\pi \sim 1$$

if $f_p^\pi \sim \frac{1}{3}$ and $f_p^\rho \sim 1$, which might be expected since the ρ's are expected to be produced indirectly by far fewer low-mass resonances. The normalization calculations in the CIM will be shown to be consistent with the prompt/total ratio of the order $50 \pm 20\%$ (see Sec. VI).

The above estimate for f_p is for a π trigger. Fewer K's are produced indirectly (especially by two-body decay), so we anticipate a somewhat smaller total/prompt ratio for K's. These ratios can certainly be determined by same-side correlation measurements. This will remove the necessity of making such rough estimates of f_p and thus will provide more stringent tests of models.

III. STRUCTURE FUNCTIONS AND CROSS SECTIONS

In this section we will present general formulas applicable to the particular reactions discussed in later sections. We will use the standard form of the hard-scattering models, where k_T integrations have already been performed.[5,7] The large-p_T cross section is then given by a convolution of structure functions $G_{a/A}(x)$ and $G_{b/B}(x)$, with the sum of all contributing hard-scattering subprocesses $a + b \to c + d$.

A. Structure functions

We begin by distinguishing between the full probability function $G_{a/A}(x)$ [for finding a particle or

system a with light-cone fraction $x=(p_a^0+p_a^3)/(p_A^0+p_A^3)$ $(p_A^T=0,\ p_A^3>0)$ in particle A] and its valence part $G^V_{a/A}(x)$ arising from the simplest valence Fock space component (2 or 3) quarks of A. Note that the complete structure function $G_{a/A}$ has the usual $x^{-\alpha(0)}$ Regge behavior, whereas the valence components vanish at $x\to 0$. In this paper we define valence quarks to refer to quarks belonging to the minimal Fock state component, and which give the leading behavior as $x\to 1$. We refer to the higher Fock components as the sea.

We constrain the G's to satisfy the spectator counting rules[6] as $x\to 1$ (see Sec. XI) and to have a reasonable shape for small x (i.e., some flattening off in xG). A form (Fig. 1) with these properties which yields simple integrals in later calculations is

$$xG_{a/A}(x)=(1+g_a)f_{a/A}N(a/A)(1-x)^{g_a},\quad x>\hat{x}_a$$
$$xG_{a/A}(x)=(1+g_a)f_{a/A}N(a/A)(1-\hat{x}_a)^{g_a},\quad x<\hat{x}_a \tag{3.1}$$

where

$$g_a=2n(\bar{a}A)-1$$

and $n(\bar{a}A)$ is the minimum number of quarks in the spectator system. We emphasize that the form (3.1) is only to be used in integrands and does not represent the true shape of the structure functions. The quantity $f_{a/A}$ is the fraction of total momentum

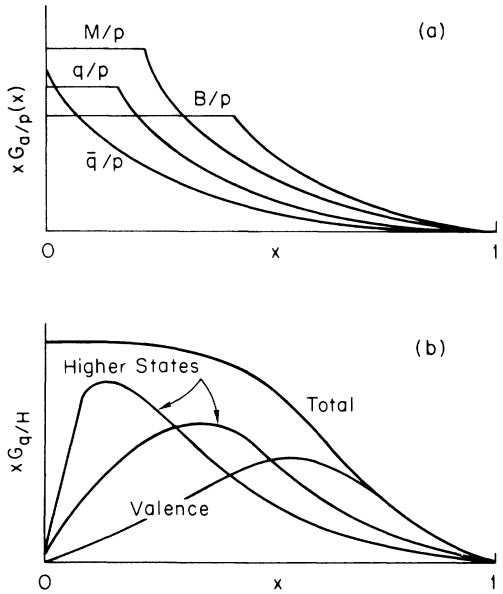

FIG. 1. (a) A schematic of the simplified structure functions used to estimate rates in the text. (b) The manner in which the higher Fock states enter to produce the total structure function.

TABLE II. Distribution-function parameters (per color).

$xG_{a/A}(x)=(1+g_a)f_{a/A}N(a/A)(1-x)^{g_a}\quad (x>\hat{x}_a)$.

a/A	g_a	$\hat{x}_a$	$f_{a/A}$	$N(a/A)$
u/p	3	0.2	0.1	1.22
d/p	3	0.2	0.067	1.22
$\bar{q}/p$	7	0	0.01	1
$(2q)/p$	1	0.6	0.1	1.6
M/p	5	0.3	0.1	2.4
K^-/p	9	0	0.024	1
B/p	3	0.3	0.12	1.6
q/π	1	0.3	0.083	1.1
$\bar{q}/\pi$	1	0.3	0.083	1.1
M/π	3	0.4	0.1	2.1
$f^V_{u/p}=2f^V_{d/p}=0.04$			$f^V_{q/M}=f^V_{\bar{q}/M}=0.033$	
$\sum'_M f_{M/p}=0.1$			$\sum'_B f_{B/p}=0.16$	
$\sum_M f_{M/p}\cong 0.4$	$\sum_B f_{B/p}\cong 0.7$		$\sum_M f_{M/\pi}\cong 0.8$	
$\sum_{q=u,d} f_{q/p}=0.17$	$\sum_{\bar{q}} f_{\bar{q}/p}=0.03$		$\sum_q f_{q/\pi}=\sum f_{\bar{q}/\pi}=0.083$	
	$\sum_{(2q)} f_{(2q)/p}=0.3$			

carried by a in A,

$$f_{a/A}\equiv\int_0^1 dx\,xG_{a/A}(x) \tag{3.2}$$

and

$$N(a/A)=[(1-\hat{x}_a)^{g_a}(1+g_a\hat{x}_a)]^{-1}. \tag{3.3}$$

As an example, reasonable values for u or d quarks in a proton are $g_a=3$ and $\hat{x}_a=0.25$. $N(a/A)$ adjusts for the shape dependence of the structure function relative to a pure $(1-x)$ power and approaches 1 as $\hat{x}_a\to 0$. *Throughout this paper if "a" refers to a quark, it will be a quark of a given color.* By way of reference, the distributions measured in deep-inelastic electron scattering are color sums

$$\nu W_2(x)=\sum_{\text{colors}}\tfrac{4}{9}xG_{u/p}(x)+\cdots$$
$$=3\times\tfrac{4}{9}xG_{u/p}(x)\cdots.$$

For simplicity, we take $G_{u/p}\propto G_{d/p}$, but different distributions could be assumed.[15b]

We will give general formulas for inclusive cross sections in terms of the parametrization (3.1); to give absolutely normalized numerical results we adopt the set of "standard" values given in Table II. Again we emphasize that these values are to be used with the simplified form (3.1) inside integrals; the parameters are chosen to yield reason-

able integral properties consistent with usual structure functions. These are taken from experiment when possible and otherwise estimated in Sec. V by utilizing the convolution formula

$$G_{a/A}(x)=\sum_n{}' \int_x^1 \frac{dz}{z} G^V_{a/n}\left(\frac{x}{z}\right) G_{n/A}(z)\,. \tag{3.4}$$

Note that to avoid double counting one of the G's must be "irreducible," i.e., a valence distribution function, and the sum, $\sum'$, is restricted to nonoverlapping intermediate particle states (n) having no quarks in common. A simple integration yields

$$f_{a/A}=\sum_n{}' f^V_{a/n} f_{n/a}\,. \tag{3.5}$$

The value of $\hat{x}_a$ in (3.1) which controls the flattening of $xG(x)$ is in general expected to be less than the position of the "quasielastic" peak in x for the valence component of interest. This tends to take into account the contributions of the higher Fock states. This is illustrated in Fig. 1. For example, for $G_{u/p}$, the most likely valence value of x is $\frac{1}{3}$ and we choose $\hat{x}_a=0.25$. The resulting form for $G_{u/p}$ is close in character to the data. For $G_{B/p}$, a baryon such as Λ or n must arise from at least the five quark wave-function component of the proton and hence the most likely "valence" value of x is $\frac{3}{5}$. We chose $\hat{x}_a=0.4$ for this case. Our final results depend only weakly on the values chosen for $\hat{x}_a$.

B. Elementary exclusive cross sections and coupling definitions

In a scale-invariant theory all exclusive differential cross sections at large momentum transfers in the fixed-angle regime can be written as a sum of terms of the form

$$\frac{d\sigma}{dt}=\pi \mathfrak{D} s^{T+U-N}(-t)^{-T}(-u)^{-U}\,, \tag{3.6}$$

where $\mathfrak{D}$ contains the relevant coupling constants. This parametrization is appropriate for general processes involving quarks, gluons, and hadrons.

There are two critical coupling constants for quark-hadron scattering which we now define. These are appropriate ones when at least one of the quarks involved is off-shell:

(i) The coupling of a meson to its simplest valence two-quark component. We define a standard coupling, $g/\sqrt{3}$, of the π^+ to a u and $\bar{d}$ quark of *one color*. The $1/\sqrt{3}$ gives the correct normalization upon summing over colors. In QCD, g is proportional to the wave function at the "origin"

$$g \propto g_s{}^2 \tilde{\psi}(0)=\frac{g_s{}^2}{(2\pi)^4}\int d^4k\,\psi(k)\,, \tag{3.7}$$

where ψ is the full Bethe-Salpeter momentum-space wave function and g_s is the colored-gluon–spin-$\frac{1}{2}$-quark coupling. A careful discussion of the definition of g and $\psi(0)$, including the effects of spin, is given in Appendix B.

(ii) We also define the constant $h/\sqrt{3}$ for the coupling of the proton to its valence state, $d+(uu)$, for applications where the (uu) system has a finite range of invariant mass. The coupling is defined for a d quark with one specific color.

For simplicity we shall assume SU(3) symmetry for the couplings throughout this paper, although we expect that some breaking may be present.

The two most important cross-section prototypes for CIM applications are as follows:

(i) The process $u\pi^+\to u\pi^+$ where u has a given color. The cross section is given in Table III. The only contribution from the valence state is the $(u\bar{d})$ topology diagram where the $\bar{d}$ quark gives a pole in the u channel. The spin-averaged cross section is characterized by $N=4$, $T=0$, $U=3$, and $\mathfrak{D}=[(1/3)\times(g^2/4\pi)]^2$ for the spin average cross section.

(ii) The process $dp\to dp$, for which all Born diagrams in a renormalizable theory yield $N=6$, i.e., $p_T{}^{-12}$ behavior. In the CIM it is assumed that the most important diagrams are those in which the gluon exchanges are internal to the hadron wave functions. Two examples are shown in Fig. 2. Diagrams in which gluons are exchanged between quarks of different hadrons are not enhanced by the strong binding effects of the wave functions. The first diagram, Fig. 2(a), which we adopt as our standard form, yields (for spin-$\frac{1}{2}$ quarks)

$$\frac{d\sigma}{dt}(dp\to dp)\propto\frac{1}{s^2}\frac{s^2+t^2}{t^2u^4}\,. \tag{3.8}$$

In the diagram of Fig. 2(b) the upper vertex is not uniquely associated with either the initial or the final proton and for simplicity we discard it; its cross-section contribution

$$\propto\frac{1}{s^2}\frac{s^2+u^2}{t^2u^2} \tag{3.9}$$

is sufficiently similar to that from Fig. 2(a) that our results are not sensitive to this assumption. The other processes of Table III involving baryons are determined by crossing from the Fig. 2(a) results. These quark spin-$\frac{1}{2}$ results for $dp\to dp$ lead to an angular distribution for elastic $pp\to pp$ scattering which is in excellent agreement with experiment as will be demonstrated below. Defining standard values

$$\alpha_M=\left(\frac{1}{3}\frac{g^2}{4\pi}\right),\quad \alpha_B=\left(\frac{1}{3}\frac{h^2}{4\pi}\right), \tag{3.10}$$

we give in Table III the cross-section forms for all elementary processes of interest for quarks interacting with $J^P=0^-$ mesons and $J^P=\frac{1}{2}^-$ baryons.

TABLE III. Elementary CIM subprocesses (spin and color averaged)

$$\frac{d\sigma}{dt} = \frac{\pi \mathfrak{D}}{s^2} \times \overline{\sum} \mathfrak{M}^2$$

Subprocess	$\mathfrak{D}$	$\overline{\sum}\mathcal{M}^2$	Subprocess	$\mathfrak{D}$	$\overline{\sum}\mathcal{M}^2$
$qM \to qM$ (ut) 	α_M^2	$\frac{s}{u^3}$	$d\bar{d} \to p\bar{p}$ 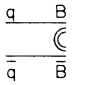	α_B^2	$\frac{s^2+u^2}{s^2t^4}$
$qM \to qM$ (st) 	α_M^2	$\frac{u}{s^3}$	$\bar{d}d \to p\bar{p}$ 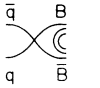	α_B^2	$\frac{s^2+t^2}{s^2u^4}$
$q\bar{q} \to M\bar{M}$ 	$\frac{1}{2}\alpha_M^2$	$\frac{u}{t^3}$	$\bar{d}p \to p\bar{d}$ 	α_B^2	$\frac{t^2+u^2}{u^2s^4}$
$Mq \to \gamma q'$ (ut) 	$2\alpha\alpha_M$	$\frac{1}{t}(s^2+u^2)\left(\frac{\lambda_{\bar{q}}}{u}-\frac{\lambda_{q'}}{s}\right)^2$	$dp \to pd$ 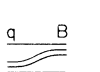	α_B^2	$\frac{s^2+u^2}{u^2t^4}$
$\gamma q \to Mq'$ (ut) 	$\alpha\alpha_M$	$\frac{1}{t}(s^2+u^2)\left(\frac{\lambda_{\bar{q}}}{u}-\frac{\lambda_{q}}{s}\right)^2$	$q(2q) \to MB$ 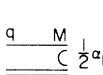	$\frac{1}{2}\alpha_B\alpha_M\alpha_D$	$\frac{u}{t^5}$
$dp \to dp$ (ut) 	α_B^2	$\frac{s^2+t^2}{t^2u^4}$	$(2q)M \to Bq$ 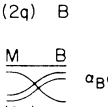	$\alpha_B\alpha_M\alpha_D$	$\frac{s}{u^5}$

One should take special note that the $\gamma q \to Mq$ cross-section form given in Table III incorporates three additional diagrams, other than the one drawn, as required by gauge invariance. All cross sections are those for quarks or diquark systems of *one given color*. The spin-$\frac{1}{2}$ quark spin-1 vector gluon structure of QCD is reflected in the tabulated results. For instance, the $qM \to qM$ cross section in a scalar quark ϕ^4 model is proportional to $1/s^2u^2$ instead of $1/su^3$ as found for spin-$\frac{1}{2}$ quarks.

C. Exclusive and inclusive hadronic cross sections

Exclusive processes

The exclusive scattering process $AB \to CD$ [see Fig. 3(a)] can be considered as the scattering of $A \to C$ off a quark constituent of the target B. Since the constituent in general has some fraction x of the target momentum, the basic subprocess occurs at a reduced energy and one readily shows from this quark-interchange diagram that

$$\frac{d\sigma}{dt}(AB \to CD) = F_{BD}^2(t) N_{\text{coh}}^2 \frac{d\hat{\sigma}}{dt}(Aq \to Cq; s' = \langle x \rangle s, t' = t, u' = \langle x \rangle u) + \text{permutations}(A, C \to B, D), \tag{3.11}$$

where the mean-value theorem has been used to replace x by $\langle x \rangle$. Note that $F_{BD}(t)$ is the full transition form factor of the target (summed over attachments to quarks of all colors) whereas $d\hat{\sigma}/dt$ is, as always, the cross section for a quark of one given color. N_{coh} is the number of coherently interfering diagrams which contribute. Using the standard form for $d\hat{\sigma}/dt$, Eq. (3.6), defining $n = 4 + N$, and taking $F_B(t) = (1 - t/M_V^2)^{-2}$ for a proton target, we obtain at large s

$$s^n \left.\frac{d\sigma}{dt}\right|_{90^\circ} = E_{\text{el}}(AB \to CD) = \pi \mathfrak{D} \langle x \rangle^{T-N} N_{\text{coh}}^2 2^{4+T+U} (M_V)^8 , \tag{3.12}$$

which is consistent with dimensional counting.[16] One expects that $\langle x \rangle \gtrsim \frac{1}{3}$ should characterize scattering from a valence component of the proton target.

Inclusive processes

From Figs. 3(a) and 3(b) it is apparent that the *direct* inclusive process, $AB \to CX$, in which the beam does *not* radiate prior to interacting with a constituent of the target, is obtained from the previously quoted exclusive scattering formula by replacing the form factor by the relevant target structure function. A simple calculation then leads

to the result

$$E_C\frac{d\sigma}{d^3p_C}(AB\to CX)=\frac{1}{\pi}\frac{s}{s+u}3\sum_{b,d}xG_{b/B}(x)\frac{d\hat{\sigma}}{dt}(AB\to Cd',\ s'=xs,\ t'=t,\ u'=xu)\,. \tag{3.13}$$

The sum of b,d is over quark flavors and the explicit 3 results from the sum over colors. The structure function G and $d\sigma/dt$ are for quarks of one given color. The variables used to describe inclusive scattering subprocess cross section $A+B\to C+X$ are

$$s+t+u=\mathfrak{M}^2=\epsilon s\,,$$

where $\mathfrak{M}$ is the total missing mass and

$$\begin{aligned}x_1&=-u/s=\tfrac{1}{2}x_R(1+z)\,,\\ x_2&=-t/s=\tfrac{1}{2}x_R(1-z)\,,\end{aligned} \tag{3.14}$$

where

$$\epsilon=1-x_R,\quad x_R\cong E^{\text{c.m.}}/E^{\text{c.m.}}_{\max}\,,$$

and $z(=\cos\theta)$ is the cosine of the center-of-mass scattering angle. The on-mass-shell condition for particle C determines x in Eq. (3.13) to be

$$x=x_2/(1-x_1)\,. \tag{3.15}$$

For $x>\hat{x}_b$ one may substitute the simple forms for $G_{b/B}$ and $d\sigma/dt$ from (3.1) and (3.6) and obtain

$$E_C\frac{d\sigma}{d^3p_C}=3\mathfrak{D}\sum_{b,d}(1+g_b)f_{b/B}N(b/B)x_1^{N-U}\times(1-x_1)^{N-T-1-g_b}K(g_b,N)\,, \tag{3.16}$$

where the dominant dynamical variation in ϵ and p_T is contained in

$$K(F,N)\equiv\epsilon^F(p_T{}^2+M^2)^{-N}\,, \tag{3.17}$$

and the effective mass scale M is less than ~1 GeV.

The double-bremsstrahlung process depicted in Fig. 4 is easily evaluated using the G functions and $d\sigma/dt$ forms already discussed. The result can be written in the form

$$E_C\frac{d\sigma}{d^3p_C}=3\sum_{a,b}I(a,b)K(F,N;F^+,F^-)J(\epsilon,z)\,. \tag{3.18}$$

Here we have employed (as appropriate for all our CIM applications) the presence of one quark-loop color sum. The sum is over the flavors of the interacting constituents. In the above formula,

$$I(a,b)=\mathfrak{D}f_{a/A}f_{b/B}N(a/A)N(b/B)2^{F^++F^-}\times\frac{\Gamma(2+g_a)\Gamma(2+g_b)}{\Gamma(2+g_a+g_b)}\,. \tag{3.19}$$

The main dynamical behavior is contained in the K function

$$K(F,N;F^+,F^-)\equiv\epsilon^F(p_T{}^2+M^2)^{-N}(1+x_Rz)^{-F^+}\times(1-x_Rz)^{-F^-}\,. \tag{3.20}$$

Note that the effective power of $\epsilon=(1-x_R)$ *changes as one approaches* $z=\pm1$. For an extension of this result to final-state decays, see Sec. IX, Eq. (9.7). In the above

$$\begin{aligned}F&=1+g_a+g_b\,,\\ F^+&=1+U+g_a-N\,,\\ F^-&=1+T+g_b-N\,.\end{aligned} \tag{3.21}$$

We have found that the function $J(\epsilon,z)$ is slowly varying in ϵ and z for $\epsilon\leq\hat{\epsilon}=1-\frac{1}{2}(\hat{x}_a+\hat{x}_b)$ and $|z|$ away from 1. In this region, it is given by

$$J(\epsilon,z)=\frac{1}{J_0}\int_{-1}^{1}d\eta(1+\eta)^{g_a}(1-\eta)^{g_b}\left[\frac{1+x_Rz+\epsilon\eta}{1+x_Rz}\right]^{-F^+}\times\left[\frac{1-x_Rz-\epsilon\eta}{1-x_Rz}\right]^{-F^-} \tag{3.22}$$

with

$$J_0=\int_{-1}^{1}d\eta(1+\eta)^{g_a}(1-\eta)^{g_b}$$

Clearly $J(0,z)=1$. In our estimates we set $J\approx1$, giving errors at most of order 20% for $\epsilon<\hat{\epsilon}$ except near the very forward or backward directions for highly asymmetric processes ($g_a\gg g_b$) where the

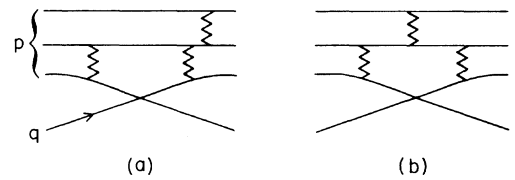

FIG. 2. Two examples of graphs that contribute to quark-proton scattering.

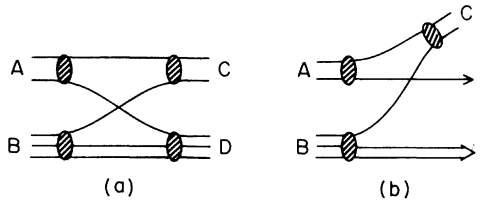

FIG. 3. (a) Typical exclusive scattering contribution to $MB\to MB$ arising from constituent interchange. (b) The corresponding inclusive direct process for $MB\to MX$ illustrating the simple connection to the structure function.

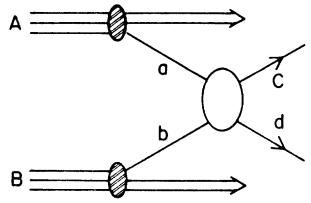

FIG. 4. The double-bremsstrahlung contribution to the prompt inclusive rate for $A+B\to C+X$. The hard-scattering contribution for the cross section is given in Eq. (1).

mean value approximations break down. The accuracy of this approximation is tested in Appendix A. The effective F power is found to decrease for $x_T < \max \hat{x}_{a,b}$.

For later use it is also convenient to define a K function that is symmetric in z,

$$K_s(F,N;F^+,F^-)=\tfrac{1}{2}[K(F,N;F^+,F^-) + K(F,N;F^-,F^+)], \quad (3.23)$$

which occurs in target-beam–symmetric (proton-proton) reactions.

IV. DETERMINATION OF COUPLING CONSTANTS FROM FIXED-ANGLE ELASTIC SCATTERING

In this section we determine the coupling constants α_M and α_B from relatively low-energy fixed-angle elastic scattering data. The values for α_M and α_B will be used later to compute the normalization of high-p_T inclusive cross sections for the CIM subprocesses. First, consider the predicted forms for photoproduction of pions and pion-nucleon and elastic scattering. Using the cross sections of Table III, with $\lambda_{\bar{q}}=\frac{1}{3}$, $\lambda_q=\frac{2}{3}$ for $\gamma u\to\pi^+ d$, we obtain from Eq. (3.12)

$$E(\gamma p\to\pi^+ n)=\pi\alpha\alpha_M\tfrac{5}{9}\langle x\rangle^{-2}2^7 M_V^8, \quad (4.1)$$

$$E(\pi p\to\pi p)=\pi\alpha_M^2\langle x\rangle^{-4}2^7 M_V^8. \quad (4.2)$$

The experimental data are consistent with[7] the predicted power laws in s. The normalization factors from Table I are

$$E(\pi p\to\pi p)=2\times10^5,$$

$$\frac{E(\gamma p\to\pi^+ n)}{E(\pi p\to\pi p)}\approx 1.3\times10^{-4}.$$

These determine $\alpha_M/\langle x\rangle^2$ in two independent ways. The effective number of coherent diagrams contributing to $\pi p\to\pi p$ is between 1 and 2. A consistent solution for both (4.1) and (4.2) is

$$\alpha_M/\langle x\rangle^2\approx 30, \quad (4.3)$$

which for $\langle x\rangle\simeq\frac{1}{4}$ gives $\alpha_M\geq 2$ GeV^2.

Now consider pp elastic scattering; there are 10 coherent diagrams as illustrated in Fig. 5. The dominant term for the basic $qp\to qp$ scattering process is given in Table III and we obtain

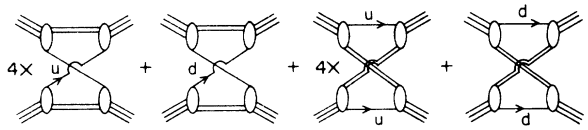

FIG. 5. The various coherent contributions to elastic proton-proton scattering and their respective weightings.

$$E(pp\to pp)=\pi\alpha_B^2\tfrac{5}{4}\langle x\rangle^{-4}N_p^2 2^{11}M_V^8. \quad (4.4)$$

Experimentally $E(pp\to pp)=1.2\times10^9$ (see Table I) and, using $\langle x\rangle\gtrsim\frac{1}{4}$, as before, one finds

$$\alpha_B\gtrsim 10\ \text{GeV}^4. \quad (4.5)$$

The CIM prediction for the quark-proton subprocess can be checked by examining the angular distribution of the pp elastic cross section about $z=\cos\theta=0$. The cross section predicted by Eq. (3.11) can be characterized by the form

$$\frac{d\sigma^{pp\to pp}}{dt}(s,z)\Big/\frac{d\sigma^{pp\to pp}}{dt}(s,0)\cong(1-z^2)^{-6}, \quad (4.6)$$

which is in good agreement with the experimental distribution.[6,7] The above form of $d\sigma/dt$ yields an effective trajectory, $\alpha(t)$, which approaches -1 as t becomes large.[17] This can also be checked by a triple-Regge analysis of $pp\to p+X$ at large t. We can also compute the ratio of the $\bar{p}p$ to pp cross sections at 90° by crossing the predicted pp form of Eq. (3.11). The CIM prediction for this ratio at 90° is

$$\frac{d\sigma}{dt}(pp\to pp)\Big/\frac{d\sigma}{dt}(\bar{p}p\to\bar{p}p)\cong 85, \quad (4.7)$$

which should be compared to the experimental ratio[18] of roughly one hundred. Models based on gluon exchange tend to give ratios of order 1. In the case of $np\to np$, there are eight rather than ten coherent diagrams, which give a predicted ratio at large angles (recall the factor of 2 for pp)

$$R=\frac{\frac{d\sigma}{dt}(np\to np)}{\frac{d\sigma}{dt}(pp\to pp)}\cong 0.32,$$

independent of s and $\theta_{\text{c.m.}}$. The data[19] for $np\to np$ and $pp\to pp$ fit the $s^{-n}f(\theta_{\text{c.m.}})$ form with $n=10.40\pm0.34$ and $n=9.81\pm0.05$, respectively, and the ratio appears to be independent of angle. These data also give $R=0.34\pm0.05$ for $10<s<24$ GeV^2, $\theta_{\text{c.m.}}=90°$. Finally, we point out that the predicted form for πp and Kp elastic scattering can be

crossed to the reaction $\bar{p}p \to \pi^+\pi^-$ and $pp \to K^-K^+$. The resultant normalization and angular distributions are in reasonable agreement with the data.[20,21]

V. DETERMINATION OF COUPLING CONSTANTS AND MOMENTUM FRACTIONS FROM MOMENTUM DISTRIBUTIONS

In this section we will use the valence distribution functions derived from deep-inelastic scattering and e^+e^- reactions to determine the quark-hadron coupling constants g and h. The valence part of the meson probability function is easily computed from the diagram of Fig. 6(a) with the result

$$G^V_{\bar{d}/\pi^+}(x) = G^V_{u/\pi^+}(x) = \int d^2k_T \frac{g^2}{6(2\pi)^3} x(1-x)[k_T^2 + M^2(x)]^{-2} = \frac{1}{3}\frac{g^2}{16\pi^2}\frac{x(1-x)}{M^2(x)}, \tag{5.1}$$

where

$$M^2(x) = (1-x)m_u^2 + xm_d^2 - x(1-x)m_\pi^2 = m_q^2 - x(1-x)m_\pi^2 .$$

We remind the reader that G^V_{u/π^+} is the distribution *per color* of quarks of flavor type u. Taking $m_\pi^2 < m_q^2$, then $M^2(x) \approx m_q^2$ and is essentially constant, so that the peak of $G^V(x)$ is at $x \sim \frac{1}{2}$. The valence component of G is unimportant at small $x < 0.5$, but it becomes dominant because of the slow $(1-x)$ falloff at large x. The e^+e^- annihilation data for single-pion production provides a direct measure of the quark-color-average (i.e., per color) distributions $G_{\pi^+/\bar{d}}$ and $G_{\pi^+/u}$. For $x \sim 0.8$ we expect that only the valence components are important, and that the crossing relation $G^V_{\pi^+/\bar{d}}(x) \sim G^V_{\bar{d}/\pi^+}(x)$ is valid for x near 1. Using the $x \sim 0.8$ data from SPEAR[22] we can estimate the coefficient of $x(1-x)$ and obtain the upper bound

$$f^V_{\bar{d}/\pi^+} = f^V_{u/\pi^+} = \int_0^1 dx\, x\, G^V_{u/\pi^+}(x) < \tfrac{1}{20}, \tag{5.2}$$

in reasonable agreement with the more detailed fits of Ellis *et al.*[23] By integrating Eq. (5.1) we find

$$\alpha_M = \frac{1}{3}\left(\frac{g^2}{4\pi}\right) = 48\pi m_q^2 f^V_{u/\pi^+}. \tag{5.3}$$

For $f^V_{u/\pi^+} = \frac{1}{30}$ and $m_q \sim 500$ MeV this yields $\alpha_M = 1.25$ GeV^2, in approximate agreement with the previous estimate of Sec. IV. (Note that m_q must be greater than $m_p/3$ for stability of the proton in our simple model in which m_q is the effective or dynamical mass of the quark.) We will adopt $\alpha_M = 2$ GeV^2 as our canonical value.

A similar calculation may be performed for the nucleon structure function. Evaluating the valence diagram of Fig. 6(b), we obtain

$$G^V_{q/B}(x) = \int_{4M_q^2}^{\infty} dD^2 \int d^2k_T \frac{h^2(D^2)}{6(2\pi)^3}\frac{x(1-x)^3}{[k_T^2 + M^2(x)]^4}, \tag{5.4}$$

where, in this case

$$M^2(x) = D^2 x + m_q^2(1-x) - x(1-x)m_p^2, \tag{5.5}$$

and D is the mass of the diquark system. Neglecting the D^2 dependence of h yields

$$G^V_{q/B}(x) = \frac{1}{3}\frac{h^2}{16\pi^2}\frac{1}{6}\frac{(1-x)^3}{[(1+3x)M_q^2 - x(1-x)M_p^2]^2}. \tag{5.6}$$

The weak x dependence of the denominator can be neglected and $G^V_{q/B}$ takes the approximate form at large x

$$G^V_{q/B}(x) \equiv 20 f^V_{q/B}(1-x)^3, \tag{5.7}$$

where $f^V_{q/B}$ is the fractional momentum carried by a valence quark of a given color. The above coefficient may be estimated from deep-inelastic scattering data for $x \sim 0.75$ yielding $f^V_{q/B} \cong (\frac{1}{3})0.12 = 0.04$. Note the similarity of this fraction to that determined in the meson case. The correct inclusion of the color factor is essential in obtaining similar valence momentum fractions for mesons and baryons. Using $m_q = 500$ MeV, as before, and thus $(1+3x)m_q^2 - x(1-x)m_p^2 \gtrsim 0.4$ GeV^2, we determine $\alpha_B \equiv \frac{1}{3}(h^2/4\pi) \cong 10$ GeV^4 in satisfactory agreement with the estimate obtained from elastic pp scatter-

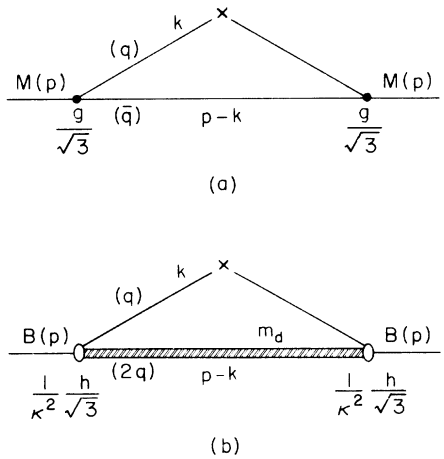

FIG. 6. The momentum routings and the couplings constants used to compute the valence contributions to the (a) meson and (b) baryon structure functions and sum rules.

ing; we adopt $\alpha_B = 10$ GeV^4 as our canonical value.

Alternatively, we can also use the asymptotic behavior of the meson and baryon form factors to determine α_M and α_B. This discussed in detail in Appendix B. The extracted values are consistent with the ones estimated above.

In addition to its valence three-quark component, the proton also contains five-quark (and higher) Fock-state components which give rise to the sea-quark distribution. In one extreme, the $qqq\ q\bar{q}$ state can be considered as a qqq baryonic system plus a $q\bar{q}$ virtual mesonlike state. Since the q and $\bar{q}$ interact over a long period of time, at least some part of the Fock state will contain color-singlet mesonic resonances.

We now turn to estimating the fraction of momentum carried by such nonoverlapping mesons in the proton and by nonoverlapping baryons in the proton. These will be crucial for the calculations of high-p_T inclusive cross sections based on hadron-quark scattering subprocesses. Some, but presumably not all, of the sea quarks can be considered as constituents of these intermediate meson systems. Using the general folding formula, Eq. (3.4), we obtain the bound

$$\sum_M {}' f^V_{\bar{d}/M} f_{M/p} \leq f_{\bar{d}/p}, \tag{5.8}$$

where the M sum runs over those nonoverlapping mesons which contain an antiquark of the given $\bar{d}$ type. Thus

$$\sum_M {}' f_{M/p} \lesssim f_{\bar{d}/p} / \langle f^V_{\bar{d}/M} \rangle, \tag{5.9}$$

where $f_{\bar{d}/p}$ and $f^V_{\bar{d}/M}$ both are per-color momentum fractions. Deep-inelastic neutrino scattering data indicate that $\sum_{\text{colors}} f_{\bar{d}/p} \sim 3 f_{\bar{d}/p} \leq 0.03$. For $f^V_{\bar{d}/M}$ we use our earlier estimate of $\frac{1}{30}$, thus yielding $\sum' f_{M/p} \lesssim 0.3$. We will use

$$\sum_M {}' f_{M/p} \approx 0.1$$

as a typical value since all $\bar{d}$'s need not come from the intermediate mesons. This value will be found to be consistent with the inclusive large-p_T data. For the $f_{B/p}$ case, the same arguments yield

$$\sum_B {}' f_{B/p} \leq f^{\text{sea}}_{q/p} / \langle f^V_{q/B} \rangle, \tag{5.10}$$

where the nonoverlapping virtual baryons B containing the quark of type q (of a given color) in a nonvalence Fock state are summed over. Again we employ $f^{\text{sea}}_{q/p} \leq 0.01$ and our earlier value $\langle f^V_{q/B} \rangle \sim 0.04$ (estimated from large-x deep-inelastic data) to obtain $\sum' f_{B/p} \lesssim 0.25$. Our nominal choice is

$$\sum_B {}' f_{B/p} \approx (\tfrac{2}{3}) 0.25 \sim 0.17.$$

When computing the high-p_T inclusive cross sections one must sum over all the intermediate mesons which can interact in the hard-scattering subprocesses $Mq \to Mq$. For example, in the proton Fock state $(uud\ \lambda\bar{\lambda})$, each of the virtual meson states $u\bar{\lambda}$, $u\lambda$, $d\bar{\lambda}$, $\lambda\bar{\lambda}$ will initiate a high-p_T $Mq \to Mq$ reaction. However, the restricted sum $\sum' f_{M/p}$ is the fraction of momentum carried by only one of the above. We will incorporate this factor of 4 by defining the "unrestricted" sum

$$\sum_M f_{M/p} \simeq 4 \sum_M {}' f_{M/p} \sim 0.4. \tag{5.11}$$

Similarly, we estimate a similar factor of 4 for the unrestricted baryon momentum sum, and adopt the value

$$\sum_B f_{B/p} \simeq 4 \sum {}' f_{B/p} \sim 0.7. \tag{5.12}$$

Notice that because the same quark momentum is counted more than once, the sum of (5.11) and (5.12) can be greater than one.

Finally, we shall need the related quantities for a pion-beam state. We estimate that

$$\sum_M f_{M/\pi} \sim 0.8.$$

When we include all Fock components of the proton or meson primary states, the usual estimate for the momentum carried by the uud quarks—summed over color—is

$$3 \sum_{q=uud} f_{q/p} = 0.5, \tag{5.13}$$

and similarly that $3 f_{u/\pi^+} = 3 f_{\bar{d}/\pi^+} = 0.25$. In each case, this implies that quarks with valence flavors carry, when all Fock states are included, one-half of the primary hadron's momentum. This then allows us to complete the entries in our Table II of standard values.

VI. INCLUSIVE CROSS SECTIONS FOR BARYON BEAMS

We have now determined all the ingredients required to predict the inclusive cross sections for specific meson, baryon, antibaryon, and photon induced reactions. We shall employ the general inclusive formulas of Sec. III, especially (3.18).

Meson production

The leading subprocesses which contribute to large-p_T inclusive reactions are those which have the mimimum p_T and $\epsilon \to 0$ falloff and the largest overall normalization. In the case of meson pro-

duction in proton-proton collisions, the dominant contributions based on quark-hadron interactions arise from quark-meson scattering ($qM^* \to qM$) and the fusion process ($q\bar{q} \to M\bar{M}^*$), which lead to the leading scaling behavior $p_T^{-8}\epsilon^9$ and $p_T^{-8}\epsilon^{11}$, respectively, for $\theta_{c.m.} \sim 90°$. The contributions from the ut diagram Fig. 7(a) and fusion diagram Fig. 7(b) yield

$$E\frac{d\sigma}{d^3p}(pp \to MX) = \alpha_M{}^2 3 \sum_{M^*q} f_{M^*/p} f_{q/p} N(M^*/p) N(q/p) 2^6 \frac{\Gamma(7)\Gamma(5)}{\Gamma(10)} K_s(9,4;5,0)$$
$$+ \tfrac{3}{2}\alpha_M{}^2 \sum_{q,\bar{q}\in M,\bar{M}^*} f_{\bar{q}/p} f_{q/p} N(\bar{q}/p) N(q/p) 2^7 \frac{\Gamma(9)\Gamma(5)}{\Gamma(12)} K_s(11,4;7,-1)$$
$$+ \tfrac{3}{2}\alpha_M{}^2 \sum_{\bar{q},q\in M,\bar{M}^*} f_{\bar{q}/p} f_{q/p} N(\bar{q}/p) N(q/p) 2^7 \frac{\Gamma(9)\Gamma(5)}{\Gamma(12)} K_s(11,4;3,3). \qquad (6.1)$$

The antiquark of the produced meson in the $qM^* \to qM$ subprocess may come from any secondary meson in the proton containing the correct antiquark flavor. This is precisely the restriction under which we derived the $\sum f_{M^*/p}$ quoted in Table II. The allowed q's to leading order are those which are in the valence state, e.g., for $M = K^+$ only $q = u$ contributes with $3f_{u/p} = 0.1 \times 3 = 0.3$.

In the $q\bar{q} \to M\bar{M}^*$ term the q and $\bar{M}^*$ sums are not independent since for a given q only certain M^*'s are present. We estimate 3 to 4 $\bar{M}^*$'s corresponding to one spin-0 and roughly three spin-1 states of given quark composition. The result at 90°, for *prompt* π^+, from the $qM \to qM$ plus fusion graphs is

$$E\frac{d\sigma}{d^3p}(pp \to \pi^+ x) = K(9,4)[4.5 + 0.10n(\bar{M}^*)\epsilon^2], \qquad (6.2)$$

where $n(\bar{M}^*)$ is the number of states in the $\bar{M}^*$ sum (~3 to 4). This equation includes the contribution from the st topology diagram of Fig 7(c) which has the angular distribution $K_s(9,4;1,0)$; at 90° it contributes only $\frac{1}{4}$ of that of the dominant ut contribution. The corrections expected from the $J(x_T)$ factor are evaluated in Appendix A.

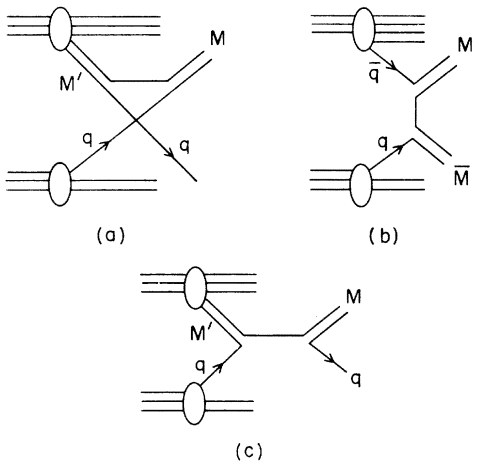

FIG. 7. Various contributions to $pp \to MX$ reactions. (a) The (ut) graph for the $qM \to qM$ basic process. (b) The corresponding inclusive direct process for $MB \to MX$ illustrating the simple connection to the structure function.

The cross section predicted above is for a prompt π^+ produced directly by the subprocess; before comparing with experiment we must allow for resonance-decay processes. In Sec. II we used the x_E distribution to estimate that $\sim\frac{1}{3}$ of the detected pions are "prompt." The data from the Chicago-Princeton group[1] give a fit of the form $p_T{}^{-n}(1-x_T)^F$ with $n = 8.2$ and $F = 9.0$, consistent with the predicted powers. Hence, *the experimental rate is roughly 9K(9,4), compared to the prediction of 13.5K(9,4).* We note that at large $x_T \to 1$, the resonance-decay contributions will increase the effective F power (by about 1 unit). However, for $x_T \sim \hat{x}$, the flattening of the structure functions (relative to a pure power) tends to compensate this small rise. See also Table V in Appendix A for a discussion of the general accuracy of the leading-power analysis.

In the SU(3)-symmetric limit the $pp \to K^+X$ cross section for prompt mesons is the same as that for the prompt π^+. However, more π^+'s than K^+'s are likely to arise from resonance decay, and in addition some SU(3) breaking is expected, hence, we expect $K^+/\pi^+ < 1$. The experimental rate is consistent with $K^+/\pi^+ \sim \frac{5}{9}$. The rate for π^- production is somewhat smaller than for π^+ since $G_{u/p}/G_{d/p}$ appears to increase as x increases.[15b] The π^+ and π^- rates must be equal, however, at $x_T = 0$, in the Feynman scaling limit, so the π^+/π^- ratio must decrease as x_T decreases to zero. As x_T increases, however, it should *rise and saturate* to a constant value in the symmetric quark model.

The dominant K^- cross section for $\epsilon \to 0$ arises from the fusion term of Eq. (6.2) and, for $n(M^*) = 4$,

$$E\frac{d\sigma}{d^3p}(pp \to K^- X)_{\epsilon} \simeq_0 0.15K(11,4). \qquad (6.3)$$

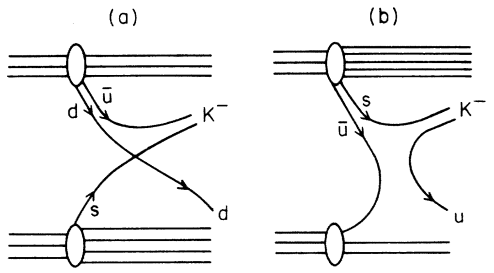

FIG. 8. The two dominant contributions to the ϵ^{13} term in the $pp \to K^- X$ yield; (a) the strangeness arising from the target and (b) the beam.

However, for moderate ϵ it is vital to retain various contributions with higher ϵ powers, for example ϵ^{13}, arising from the *ut* and *st* topology $qK^- \to qK^-$ graphs of Fig. 8. Each contributes a prompt cross section of approximately (at 90°)

$$\sim 0.7K(13,4). \tag{6.4}$$

For Fig. 8(b) the K^- distribution inside a proton is normalized by taking $G_{K^-/p}(x) = G_{K^+/p}(x)$ at $x \to 0$ (see Table II). Related higher Fock space state graphs for K^+, π^+ production have already been included via the full $G_{u/p}$ quark distribution and $G_{M/p}$ meson distribution functions, which represent sums over all Fock space components starting with the minimal one. Our estimate for the K^-/K^+ ratio is thus

$$\frac{d\sigma(pp \to K^-)}{d\sigma(pp \to K^+)} = 0.03\epsilon^2 \frac{1+4.6\epsilon^2}{1+0.1\epsilon^2} \simeq 0.03\epsilon^2(1+4.5\epsilon^2). \tag{6.5}$$

Recall that the numerical approximations used are not valid for $\epsilon \to 1$. Experimentally, this ratio has the same shape as the above prediction but with about four times the magnitude. One sees that the fusion term dominates only for $x_T > 0.6$.

If the total/prompt ratio for K^- is larger than for K^+, (6.5) will be closer to the experimentally observed ratio of total rates. We are not at liberty to increase the fusion contribution since to decrease $\sum f_{M/p}$ [see Eq. (5.9)] and therefore, presumably, $\sum f_{M/\pi}$ and $\sum f_{B/p}$ (thereby decreasing the K^+ but not the K^- cross section) would destroy the meson beam normalizations of the next section and the baryon production predictions discussed below. Increasing $f_{\bar{q}/p}$ significantly would also not be consistent with deep-inelastic neutrino data.

We have, in the preceding meson yield calculations, ignored the quark-diquark fusion diagrams. We will now show that their contribution to meson production is small. For $q(qq) \to K^+ B^*$ we have

$$E\frac{d\sigma}{d^3p} = \tfrac{1}{2}\alpha_B \alpha_M \alpha_D 3 f_{u/p} \sum f_{(qq)/p} n(B^*) N(q/p) N(qq/p) \times \frac{\Gamma(5)\Gamma(3)}{\Gamma(6)} K(5,6)$$

$$\sim 0.4 n(B^*) K(5,6).$$

In order to make this estimate we have assumed that the parameter α_D, obtained by integrating over the diquark internal momenta, is of order $\alpha_M \sim 1$ GeV^2.

For $p_T > 2$ GeV/c this contribution is very small compared to the $qM \to qM$ contributions unless ϵ is quite close to zero. However, it could be an important contribution to double-trigger experiments on a meson-baryon pair. We note that charge correlations between the trigger and fast away-side particles can be an important discriminant of the contributing subprocesses. We discuss this further in Sec. XI.

Before leaving the discussion of meson yields let us apply our estimates to the production of high-p_T *pions from antiproton beams*. Using the general formula (3.18) one sees that only the second term of Eq. (6.1) has to be modified. Since the antiquark distribution in the antiproton is the same as quarks in a proton, one has to multiply the second term of Eq. (6.2) by the factor

$$(33/2^4 7\epsilon^4)(f_{\bar{q}/p} N_{\bar{q}/p})/[f_{\bar{q}/p} N(\bar{q}/p)] \cong 1/\epsilon^4.$$

The predicted ratio of meson yields from antiproton and proton beams then becomes

$$\frac{d\sigma(\bar{p}p \to \pi x)}{d\sigma(pp \to \pi x)} = \frac{1+0.02n(\overline{M}^*)\epsilon^{-2}}{1+0.02n(\overline{M}^*)\epsilon^2} \cong 1+0.08(\epsilon^{-2}-\epsilon^2), \tag{6.6}$$

using $n(\overline{M}^*) = 4$. For example, at $x_T = 0.3$, the ratio is predicted to be 1.20. In quark-scattering models, it should be unity, thus there is not much difference until x_T is large. In a model with fusion only, the ratio would be ϵ^{-4}, which is 4 at $x_T = 0.3$.

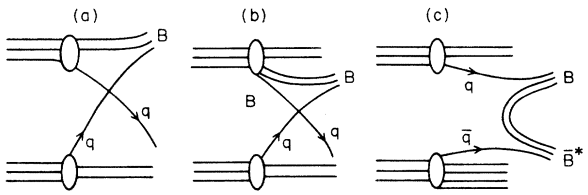

FIG. 9. Baryon production from proton beams; (a) the direct-scattering graph, (b) beam bremsstrahlung (of a mesonic spectator system), and (c) the fusion process, are shown.

Baryon production

The dominant contributions in the CIM for $p+p \to p+X$ at high p_T arise from the basic subprocesses $Bq \to pq$ and $q\bar{q} \to p\bar{B}^*$. The first process includes the direct contribution $pq \to pq$ in which the incident proton participates in the hard-scattering subprocess, as in Fig. 9(a). Using our general formulas, (3.16) and (3.18), the inclusive cross section is

$$E\frac{d\sigma}{d^3p}(pp \to px) = \alpha_B{}^2 3 \sum_q 4 f_{q/p} N(q/p) x_1{}^2 2K(3,6)$$
$$+ \alpha_B{}^2 3 \sum_{B,q} f_{q/p} f_{B/p} N(q/p) N(B/p) 2^3 \frac{\Gamma(5)\Gamma(5)}{\Gamma(8)} K_s(7,6;2,0)$$
$$+ \alpha_B{}^2 3 \sum_{\bar{q}q,\bar{B}^*} f_{q/p} f_{\bar{q}/p} N(q/p) N(\bar{q}/p) 2^5 \frac{\Gamma(5)\Gamma(9)}{\Gamma(12)} K_s(11,6;-2,6). \tag{6.7}$$

Note that the two up quarks contribute coherently in the proton cross section. These are the contributions with leading $\epsilon \to 0$ behavior. All valence quarks participate in p production; thus $3\sum f_{q/p} \simeq 0.5$. Also, from Sec. V, $\sum f_{B/p} \sim 0.7$. At 90° the cross-section prediction for *prompt protons* is then

$$E\frac{d\sigma}{d^3p}(pp \to pX) = 342 x_T{}^2 K(3,6)$$
$$+ 394K(7,6) + 4.2n(\bar{B}^*)K(11,6), \tag{6.8}$$

where, in common with the fusion process for mesons, we estimate $n(\bar{B}^*) \sim 3$–4. The last term is never large, and for $x_T = 1-\epsilon \lesssim 0.4$, the indirect term $K(7,6)$ dominates. The direct (leading-particle) term dominates the indirect $qB \to qp$ term when $x_T > 0.5$. Present data are reasonably fitted by $500\,K(7,6)$ implying a prompt-to-total ratio for protons of roughly 80%, greater than for pions.

The $q(qq) \to M^* p$ contribution is also easily estimated by slightly altering the earlier π^+ production result. One finds

$$\sim 0.7 n(M^*) K(5,6).$$

It is clear that this term is much smaller than the $qB \to qp$ contributions for reasonable ϵ.

The *prompt antiproton* yield from the fusion $q\bar{q} \to \bar{p}B^*$ term is

$$E\frac{d\sigma}{d^3p}(pp \to \bar{p}x) = 11K(11,6), \tag{6.9}$$

with the total yield about three times larger. For $x_T < \frac{1}{2}$, however, it is certainly necessary to include terms for $\bar{p}$ production with higher ϵ powers. In particular, one obtains a large $p_T{}^{-12}\epsilon^{15}$ term from $\bar{p}q \to \bar{p}q$ scattering. The situation is as for K^- production: The fusion term (6.9) only dominates for small ϵ, i.e., at the edge of phase space.

Comparison of γ and π^0 yields

From our previously developed general equations, one finds at 90°

$$E\frac{d\sigma}{d^3p}(pp \to \gamma X) = \frac{5}{2}\alpha\,\alpha_M 3 \sum_{M,q} f_{M/p} f_{q/p} (\lambda_{\bar{q}} - \tfrac{1}{2}\lambda_{q'})^2$$
$$\times N(M/p) N(q/p) 2^8$$
$$\times \frac{\Gamma(7)\Gamma(5)}{\Gamma(10)} K(9,3), \tag{6.10}$$

where we identify $\lambda_{\bar{q}} = -\lambda_q$ and $\lambda_{q'} = \lambda_M - \lambda_{\bar{q}}$ by using the $Mq \to \gamma q'$ subprocess for prompt photons shown in Fig. 10(a). Thus the photon cross section is predicted to scale as $p_T{}^{-6}(1-x_T)^9$ at $\theta_{\text{c.m.}} = 90°$. For π^0 production, on the other hand, we have

$$E\frac{d\sigma}{d^3p}(pp \to \pi^0 x) = \tfrac{1}{2}\alpha_M{}^2 3 \sum_{M,q} f_{M/p} f_{q/p} N(M/p) N(q/p)$$
$$\times 2^6 \frac{\Gamma(7)\Gamma(5)}{\Gamma(10)} K_s(9,4;5,0), \tag{6.11}$$

where the explicit $\frac{1}{2}$ accounts for $\pi^0 = (\frac{1}{2})^{1/2}(u\bar{u} - d\bar{d})$ composition. The γ/π^0 ratio at 90° is (after multiplying the above π^0 yield by the total/prompt ~3 ratio)[24]

$$\frac{d\sigma(pp \to \gamma)}{d\sigma(pp \to \pi^0)} \cong \frac{2}{3}\frac{5\alpha}{3\alpha_M}(p_T{}^2 + M^2)$$
$$\sim 0.004(p_T{}^2 + M^2). \tag{6.12}$$

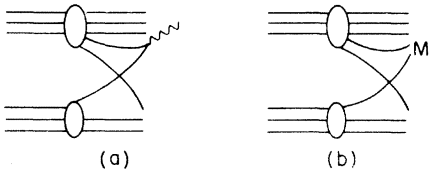

FIG. 10. Illustrating the simple and direct relation between (a) photon and (b) meson production for one type of basic process.

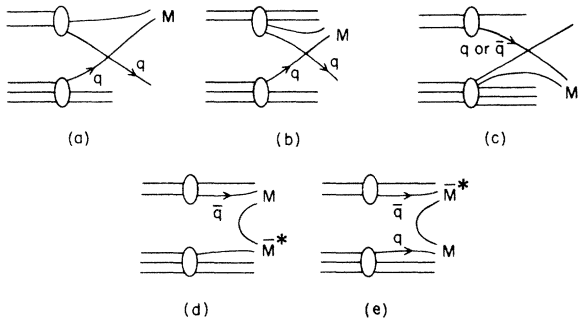

FIG. 11. The five important contributions to meson production by meson beams. The direct process is (a), and the quark-meson process in which the intermediate meson arises from the (b) incident meson and (c) proton target are also shown. The two possible fusion processes are shown in (d) and (e).

This is less than $\frac{1}{2}$ the preliminary ratio reported by Darriulat *et al.*,[12] at $p_T \sim 3$ GeV/c. However, there are other CIM sources of photons, giving a p_T^{-8} scaling behavior, from bremsstrahlung processes as well as from π^0 and η decay. These should give a roughly constant contribution to the γ/π ratio.

The $Mq \to \gamma^* q$ subprocess with the same normalizations has been used in Ref. 24a to successfully describe the p_T falloff of massive lepton pairs from proton and pion beams. Thus these normalizations are consistent with those of the Drell-Yan process.

VII. INCLUSIVE CROSS SECTIONS FOR PION BEAMS

In this section, the inclusive production of mesons, baryons, and antibaryons at large transverse momentum by pion beams will be discussed. The comparison of yields from pion and proton beams is a very important constraint on any model and on the values of the parameters used to describe the data.

The meson yield from a pion beam arises in the CIM from the five dominant diagrams illustrated in Fig. 11, corresponding to the direct basic process, $M^*q \to Mq$ (where the M^* can arise from the beam or target), $M^*\bar{q} \to M\bar{q}$, $\bar{q}q \to M\bar{M}^*$, and $\bar{q}q \to \bar{M}^*M$. Not all of these contribute to the yield of all mesons. For example, there is no direct diagram for the K^- yield from a pion beam. The respective contribution of these terms to the inclusive cross section easily follows from our general formula

$$E\frac{d\sigma}{d^3p}(\pi p \to MX) = \alpha_M{}^2 3 \sum_q f_{q/p} N(q/p) x_1 4K(3,4) + \alpha_M{}^2 3 \sum_{q,M^*} f_{q/p} f_{M^*/\pi} N(q/p) N(M^*/\pi) \frac{2^3\Gamma(5)\Gamma(5)}{\Gamma(8)} K(7,4;3,0)$$
$$+ \alpha_M{}^2 3 \sum_{q,\bar{q},M^*} (f_{q/\pi} + f_{\bar{q}/\pi}) f_{M^*/p} N(q/\pi) N(M^*/p) \frac{2^3\Gamma(3)\Gamma(7)}{\Gamma(8)} K(7,4;-2,5)$$
$$+ \tfrac{1}{2}\alpha_M{}^2 3 \sum_{q,\bar{q},M^*} f_{q/p} f_{\bar{q}/\pi} N(q/p) N(\bar{q}/\pi) \frac{\Gamma(3)\Gamma(5)}{\Gamma(6)} [K(5,4;1,-1) + K(5,4;-3,3)]. \quad (7.1)$$

The sums are restricted according to the quantum number of the produced meson (e.g., only $q = d$ contributes for the direct contribution to $\pi^+ p \to \pi^0 X$).

If we take $\sum f_{M^*/\pi} \sim \sum f_{B^*/p} \sim 0.8$ then this formula gives for π^0 production (including the factor of $\frac{1}{2}$ for the $\pi^0 \to d\bar{d}$, $u\bar{u}$ coupling) at 90°

$$E\frac{d\sigma}{d^3p}(\pi^+ p \to \pi^0 X) = 1.4 x_T K(3,4)$$
$$+ K(7,4)[4.7] + K(5,4)[0.04] n(\bar{M}^*)$$
$$= K(7,4)[4.7 + 0.04 n(\bar{M}^*)\epsilon^{-2}$$
$$+ 1.4 x_T \epsilon^{-4}]. \quad (7.2)$$

The corrections from $J(x_T)$ are evaluated in Appendix A, Table V. The most important contribution for $x_T < 0.4$ is the $K(7,4)$ term which arises from meson-quark scattering. For $n(\bar{M}^*) = 4$ the fusion term dominates the M-q term for $x_T \gtrsim 0.8$. The direct $\pi^+ q \to \pi^0 q$ term dominates the indirect $qM \to qM$ contribution when $x_T \gtrsim 0.5$. The present experimental results are compatible with the fit $3.5K(7,4)$ for $x_T \lesssim 0.5$, confirming that the direct term does not dominate in that region. We predict that a transition should appear in the data: Near 90°, as x_T increases above ≈ 0.5, the $d\sigma \sim \epsilon^7 p_T^{-8}$ behavior will change to a $d\sigma \sim \epsilon^3 p_T^{-8}$ behavior. The occurrence of such a transition is an important test of the normalization and dynamics of the CIM approach.

For small x_T, the direct and annihilation terms can be neglected in Eq. (7.2) to yield a simplified result. In the same region of x_T, the prediction for $pp \to \pi^0$ is also simple and one finds that the ratio is expressible as [taking $N(M/p) \sim N(M/\pi)$]

$$\frac{d\sigma(\pi^+ p \to \pi^0)}{d\sigma(pp \to \pi^0)} = \epsilon^{-2}\frac{3}{4}\frac{\sum_q [(f_{q/\pi} + f_{\bar{q}/\pi}) N(q/\pi) + \frac{2}{5} f_{q/p} N(q/p)]}{\sum_q f_{q/p} N(q/p)}. \quad (7.3)$$

The momentum fraction $f_{M/p}$ has canceled as well

as $\alpha_M{}^2$ and the prompt/total ratio. The experimental value[2] for the above ratio is roughly $\sim 0.6\epsilon^{-2}$, whereas Eq. (7.3) predicts $\sim 1.0\epsilon^{-2}$. Corrections to this ratio and to the difference in effective F powers are given in Appendix A. Chase and Stirling (Ref. 6) have also predicted a ratio similar to (7.3). We do not consider the present discrepancy to be serious.

Let us now turn to predictions for two reactions which have not yet been measured, namely $\pi p \to pX$ and $\pi p \to \bar{p}X$. The first reaction has several important terms, which are illustrated in Fig. 12. These five contributions [(a)–(e)] scale as $p_T{}^{-12}$ at fixed ϵ and $\theta_{\text{c.m.}}$ and take the form respectively

$$
\begin{aligned}
E\frac{d\sigma}{d^3\sigma}(\pi p \to p) = {} & \alpha_B{}^2 3 \sum_q f_{q/\pi} N(q/\pi) x_2{}^2 (1-x_2)^2 [1+(1-x_2)^2] 2K(1,6) \\
& + \alpha_B{}^2 3 \sum_q f_{\bar{q}/\pi} N(\bar{q}/\pi) [x_2{}^6 (1-x_2)^4 + x_2{}^8 (1-x_2)^2] 2K(1,6) \\
& + \alpha_B{}^2 3 \sum_{q,B^*} f_{q/\pi} f_{B^*/p} N(q/\pi) N(B'/p) \frac{\Gamma(3)\Gamma(5)}{\Gamma(6)} K(5,6;0,0) \\
& + \alpha_B{}^2 3 \sum_{\bar{q},B^*} f_{\bar{q}/\pi} f_{B^*/p} N(\bar{q}/\pi) N(B'/p) 2^{-4} \frac{\Gamma(3)\Gamma(5)}{\Gamma(6)} K(5,6;-2,-2) \\
& + \alpha_B{}^2 3 \sum_{q\bar{q},\bar{B}*} f_{\bar{q}/\pi} f_{q/p} N(\bar{q}/\pi) N(q/p) 2^{-2} \frac{\Gamma(3)\Gamma(5)}{\Gamma(6)} K(5,6;0,-2) .
\end{aligned} \tag{7.4}
$$

Using the nominal values of the constants this cross section becomes at 90° (again note that u-quark contributions are coherent)

$$
\begin{aligned}
E\frac{d\sigma}{d^3p}(\pi^+ p \to p) = {} & 55 x_T{}^2 (1-\tfrac{1}{2}x_T)^2 \\
& \times [1+(1-\tfrac{1}{2}x_T)^2] K(1,6) \\
& + 110 K(5,6) ,
\end{aligned} \tag{7.5}
$$

where $n(\bar{B}^*) \sim 4$ is the estimated number of baryon resonances of a given quark composition. These two terms become comparable for $x_T \sim 0.3$ with the second term dominating for smaller x_T. For this latter region of small x_T, if only the dominant terms are retained, the π/p yield at $\theta_{\text{c.m.}} = \pi/2$ takes the simple form

$$
\begin{aligned}
\frac{d\sigma(\pi p \to \pi)}{d\sigma(\pi p \to p)} = {} & \frac{\alpha_M{}^2}{\alpha_B{}^2} \epsilon^2 (p_T{}^2 + M^2)^2 \frac{2^6 \times 5}{7} \\
& \times \frac{\sum_M f_{M/p} N(M/p)}{\sum_B f_{B/p} N(B/p)}
\end{aligned} \tag{7.6}
$$

This ratio can be used to check a new combination of the couplings used in the model. Using our nominal values, this becomes

$$
= 0.75\epsilon^2 (p_T^2 + M^2)^2 , \tag{7.7}
$$

where we expect $M^2 \lesssim 1$ GeV^2.

The antiproton yield with leading ϵ power arises from the last term only, the fusion graph. The general formula is

$$
\begin{aligned}
E\frac{d\sigma}{d^3\bar{p}}(\pi^+ p \to \bar{p}) = {} & \alpha_B{}^2 n(B^*) 3 \\
& \times \sum_{\bar{q},q} f_{\bar{q}/\pi} f_{q/p} N(\bar{q}/\pi) N(q/p) 2^{-2} \\
& \times \frac{\Gamma(3)\Gamma(5)}{\Gamma(6)} K(5,6;-4,2)
\end{aligned} \tag{7.8}
$$

and at 90°, the nominal value is

$$
= 1.2 n(B^*) K(5,6)
$$

Using $n(B^*) = n(\bar{B}^*) \cong 4$ as a nominal value, the ratio of the $\bar{p}$ yield to the p yield for small x_T at 90° is

$$
\frac{d\sigma(\pi p \to \bar{p})}{d\sigma(\pi p \to p)} = 0.04[\tfrac{1}{4} n(B^*)] . \tag{7.9}
$$

As for K^- and $\bar{p}$ production in proton beams, important background contributions with higher ϵ powers are expected, and these can be estimated in the same manner as before.

VIII. INCLUSIVE-EXCLUSIVE CONNECTION

In the limit $\epsilon \to 0$, a direct inclusive process such as that for Fig. 3 is expected to smoothly connect to its corresponding exclusive process, in this case Fig. 3(a). Following Bjorken and Kogut[25] this can be made quantitative by integrating the inclusive cross section over a finite range in missing mass:

$$
\begin{aligned}
\frac{d\sigma^{\text{inc}}}{dt} \equiv {} & \frac{\pi}{s} \int_{\Delta \mathfrak{M}^2} d\mathfrak{M}^2 E \frac{d\sigma}{d^3p} \\
= {} & \int_{\Delta \mathfrak{M}^2} d\mathfrak{M}^2 \frac{d\sigma}{dt d\mathfrak{M}^2} .
\end{aligned} \tag{8.1}
$$

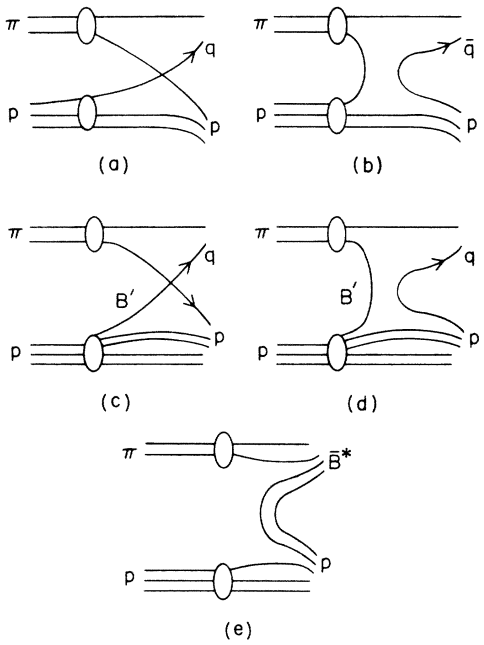

FIG. 12. The five dominant contributions to baryon (and antibaryon) production by meson beams.

Using our general formula, Eq. (3.16), for direct processes, we obtain for a proton target

$$E_{\rm inc}\equiv s^{N+4}\frac{d\sigma^{\rm inc}}{dt}=\pi\mathfrak{D}3\sum_q f_{q/p}N(q/p)2^{6+T+N}\times\int_{\Delta\mathfrak{M}^2}d\mathfrak{M}^2(\mathfrak{M}^2-M_p^{\,2})^3.$$

Using the definition of E_{el}, Eq. (3.12), the ratio between inclusive and exclusive scattering becomes

$$\frac{E_{\rm inc}}{E_{\rm el}}=12\sum_q f_{q/p}N(q/p)\frac{\langle x\rangle^{N-T}}{M_V^{\,8}}\int_{\Delta\mathfrak{M}^2}d\mathfrak{M}^2(\mathfrak{M}^2-M_p^{\,2})^3. \tag{8.2}$$

Now let us apply this to π^+p and pp scattering. For both of these processes, $N-T=4$. In addition, since M_V measures the rate of falloff of the nucleon form factor and hence provides a measure of the coherence of the proton wave function, we choose $\Delta\mathfrak{M}=M_V$, and achieve the form

$$\frac{E_{\rm inc}}{E_{\rm el}}=3\sum_q f_{q/p}N(q/p)\frac{\langle x\rangle^4}{M_V^{\,8}}[(M_p+M_V)^2-M_p^{\,2}]^4\simeq 0.8\left[\frac{3\sum_q f_{q/p}N(q/p)}{(0.5)(1.2)}\right](3\langle x\rangle)^4, \tag{8.3}$$

which indeed is of order one for our nominal values for the momentum fraction $f_{q/p}$, the shape function $N(q/p)$, and $\langle x\rangle=\frac{1}{3}$ (see Table II). Note that this comparison does not account for the coherence of various amplitudes at the exclusive limit.

IX. THE CROSSOVER BETWEEN CIM AND QUARK-QUARK SCATTERING SUBPROCESSES

As we have emphasized, subprocesses based on quark-hadron interactions must occur in any quark-parton model. In the preceding section we have shown that the magnitude of the $q\bar{q}$-M and qqq-B couplings (determined from form factors and exclusive processes) leads to inclusive high-p_T cross sections consistent with the experimentally observed normalization and scaling behavior for $p_T<8$ GeV/c. In this section we will compare the scale-invariant contribution from quark-quark scattering expected in lowest-order QCD with the CIM contributions, and we estimate the crossing point in p_T where a p_T^{-4} scaling behavior can be expected to dominate. In our calculations large scale-breaking effects in the structure functions will be assumed to be absent.[26] We also need only consider the scattering of valence quarks, since only a small fraction of the momentum of the proton is carried by sea quarks. In addition one expects scale-invariant p_T^{-4} contributions in QCD from gluon-quark and gluon-gluon interactions; these, however, require knowledge of gluon distributions which are highly model dependent. Estimates of QCD contributions are made in Ref. 8, but for completeness, we will repeat some of their discussion within our calculational framework.

The differential cross section for quark-quark scattering from the lowest-order QCD diagrams shown in Fig. 13 is[8]

$$\frac{d\sigma}{dt}(q_\alpha q_\beta\to q_\alpha q_\beta)=\frac{\pi\alpha_s^{\,2}}{s^2}\left[\frac{4}{9}\left(\frac{s^2+u^2}{t^2}+\delta_{\alpha\beta}\frac{s^2+t^2}{u^2}\right)-\frac{8}{27}\frac{s^2}{ut}\delta_{\alpha\beta}\right]. \tag{9.1}$$

This cross section is spin- and color-averaged and includes interference terms between t-channel and u-channel graphs that are present when $\alpha=\beta$. The color coupling $\alpha_s=g_s^{\,2}/4\pi$ is defined by the interaction Lagrangian

$$\mathfrak{L}_I=g_s\bar{\Psi}\gamma_\mu\tfrac{1}{2}\lambda_a\Psi A_\mu^a,\quad \mathrm{Tr}\lambda_a^{\,2}=2. \tag{9.2}$$

We will calculate jet and single-particle cross sections, but leave the discussion of the former to

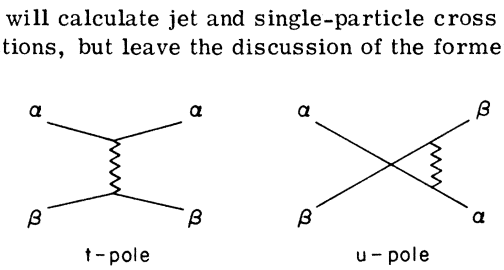

FIG. 13. Lowest-order diagrams for quark-quark scattering via gluon exchange.

the following section. For proton targets $q=u$, d dominate and we can safely neglect antiquarks and the $\bar{q}q$ scattering contributions.

In the case of the jet-trigger cross section from $q_\alpha q_\beta \to q_\alpha q_\beta$, we must distinguish carefully the cases $\alpha=\beta$ and $\alpha\neq\beta$. In the latter case the jet trigger receives a contribution from either of the final-state quarks and the cross section should be doubled. For the case $\alpha=\beta$, the cross section already accounts for both trigger possibilities. The 90° jet-trigger cross section can be computed in a convenient analytic form from Eq. (3.18). The factor which changes from term to term in this formula is $2^{F+F^-}=2^{4+T+U}$.

The various terms in the bracket of Eq. (9.1) then give

$$\tfrac{4}{9}2^4[(2^2+1)+\delta_{\alpha\beta}(2^2+1)-\tfrac{2}{3}\delta_{\alpha\beta}2^2]=\tfrac{4}{9}2^4[5+\tfrac{7}{3}\delta_{\alpha\beta}], \tag{9.3}$$

which, when weighted by the $f_{q/p}$ factors, gives

$$\tfrac{4}{9}2^4\times\begin{cases}(0.3)^2[22/3]\ uu,\\ 2(0.3)(0.2)[5]\ ud+du,\\ (0.2)^2[22/3]\ dd.\end{cases} \tag{9.4}$$

For triggering on a jet arising from either a u or a d quark we take

$$uu+2(ud+du)+dd,$$

while for a u trigger only we use

$$uu+(ud+du).$$

Thus

$$E\frac{d\sigma}{d^3p}\left(pp\to\begin{bmatrix}u\text{ or }d\\ u\text{ only}\end{bmatrix}X\right)=K(7,2)\alpha_s^2N^2(q/p)\times\tfrac{4}{9}2^4\frac{\Gamma(5)\Gamma(5)}{\Gamma(8)}\begin{bmatrix}2.15\\ 1.26\end{bmatrix}=K(7,2)\alpha_s^2\begin{bmatrix}2.51\\ 1.47\end{bmatrix}. \tag{9.5}$$

This analytic form is a useful characterization of the QCD qq jet cross section.

In order to compute the cross section for the production of a specific hadron h one must incorporate the final-state fragmentation function $D_{h/q}$:

$$E\frac{d\sigma}{d^3p}(p_1p_2\to hx)=\sum_q\int_{x_R}^1\frac{dz}{z^2}D_{h/q}(z)\times E\frac{d\hat{\sigma}}{d^3p}(p_1p_2\to q;s,t/z,u/z). \tag{9.6}$$

Using

$$D=d\frac{(1-z)^f}{z}\ \text{and}\ E\frac{d\hat{\sigma}}{d^3p}=IK(F,N), \tag{9.7}$$

we obtain at 90° [defining $z=w+(1-w)x_T$]

$$E\frac{d\sigma}{d^3p}(pp\to h)=\sum_q dIK(F+f+1,N)\hat{J}(x_T), \tag{9.8}$$

where

$$\hat{J}(x_T)=\int_0^1 dw(1-w)^fw^F[w+(1-w)x_T]^{2N-F-3}.$$

We approximate the integral using the mean-value theorem [$\langle w\rangle=F/(f+F)$] and find

$$\hat{J}\cong\frac{\Gamma(1+f)\Gamma(1+F)}{\Gamma(2+f+F)}\left(\frac{f+F}{F+fx_T}\right)^{3+F-2N}. \tag{9.9}$$

The last factor is relatively slowly varying. For typical values $f=1$, $F=7$, $N=2$, it varies from 2.3 at $x_T=0$ to 1 at $x_T=1$. For very small $x_T(<0.1)$ the above approximation is not adequate and must be supplemented.

As an example, for quarks decaying to mesons, $f=1$, Eq. (9.9) gives the suppression factor

$$\frac{\Gamma(1+f)\Gamma(1+F)}{\Gamma(2+f+F)}=\frac{1}{(1+F)(2+F)}\sim\frac{1}{F^2}.$$

For the π^+ cross section, a reasonable fit to the quark fragmentation functions gives $D_{\pi^+/u\ (\text{or}\ \bar{d})}(z)=1.0(1-z)/z$. Equation (9.8) then gives at 90°

$$E\frac{d\sigma}{d^3p}(pp\to q\to\pi^+)=K(9,2)\alpha_s^2(0.035), \tag{9.10}$$

where we evaluated $J(x_T)$ at $x_T=0.3$. The ratio of this contribution to the data (or the CIM prediction) is $0.0044\alpha_s^2p_T^4$ or $4\times10^{-4}p_T^4$ for $\alpha_s=0.3$. Thus the CIM p_T^{-8} terms can dominate the cross section for $p_T<7$ GeV/c. The crossover moves to $p_T\cong10$ GeV/c for $\alpha_s=0.15$. The above result is not sensitive to the form of $D_{h/q}$ for reasonable fits to the fragmentation data obtained from e^+e^- annihilation and deep-inelastic scattering. The total yield can be succinctly written in the form

$$E\frac{d\sigma}{d^3p}=A\left[\left(\frac{10}{p_T}\right)^8+\left(\frac{\alpha_s}{0.15}\right)^2\left(\frac{10}{p_T}\right)^4\right]\epsilon^9, \tag{9.11}$$

which may prove convenient in fitting the large-p_T data. Equation (9.11) implies for $\alpha_s=0.15$ a change in the p_T power (at fixed ϵ) from $n_{\text{eff}}=7.5$ at $p_T=6$ to $n_{\text{eff}}=4.8$ at $p_T=14$ GeV/c.

X. JET-JET CROSS SECTIONS

We turn now to the calculation of the cross section for jet production at large transverse momentum obtained from the CIM hard-scattering subprocesses. In the CIM the jets consist of single hadrons, multiparticle resonances, as well as quark and antiquark jets which arise from subprocesses such as $Mq\to Mq$, $Bq\to Bq$, and $M\bar{M}\to q\bar{q}$. We shall also make comparisons with the jet-trigger cross sections calculated from quark-quark scattering in Sec. IX. It should be emphasized that

the relationship of the predicted jet cross sections may not be simply related to what is measured experimentally in calorimeter trigger experiments, due to the effects of resolution, background particles, and missed hadrons. Furthermore, there may well be contributions from multiple-scattering processes or multiple high-p_T reactions in the same event which can complicate the jet trigger.

Let us now estimate the jet-jet cross section in pp collisions. In the CIM, the cross section for producing a single prompt meson or proton is expected to be $\frac{1}{4}$ to $\frac{1}{2}$ the observed inclusive cross section. The remainder is made up by production of resonances which decay into the observed meson. In a jet trigger all the decay products of a given resonance are seen which effectively means that we must multiply our prompt cross sections by the number of possible resonances. In addition, a jet trigger also can catch the decay products of the quark which normally balances the trigger meson in the CIM diagrams. We proceed to quantitatively estimate these effects (discussing only those diagrams which are important).

The important subprocesses are as follows:

(a) $Mq \to M^*q$. Either M^* or q may be the jet. We estimate the number of M^*'s which can participate as $N(M^*) \geq 9 + 3\times 9 = 36$ corresponding to the spin-0 and spin-1 mesons nonets with statistical weighting. In support of this we cite the ρ cross section which experimentally is approximately equal to the *total* π cross section.[15] Since more ρ's are presumably prompt as compared to the pions (not decay products of still higher resonances), we are led to (see also Ref. 14)

$$\frac{\pi(\text{prompt})}{\rho(\text{prompt})} \approx \frac{\frac{1}{3}\pi(\text{total})}{\rho(\text{total})} \sim \frac{1}{3}.$$

In the following we take $N(M^*) = 40$ as a reasonable estimate; note that the previously employed $n(M^*)$ is that portion of $N(M^*)$ resonances which can be produced by quarks *of a given type*, i.e., $n(M^*) \simeq \frac{1}{9}N(M^*) \simeq 3$–$4$.

Including both the quark jet and meson-resonance trigger, we have, for $qM \to qM^*$,

$$E\frac{d\sigma}{d^3p}(pp \to jet(\text{meson induced})) \approx 80E\frac{d\sigma}{d^3p}(pp \to \pi(\text{prompt})) \approx 27E\frac{d\sigma}{d^3p}(pp \to \pi(\text{total})). \quad (10.1)$$

The above prompt ratio of $\frac{1}{3}$, as discussed in Sec. II, also leads to reasonable x_E distributions: dN/dx_E must extend beyond $x_E = 1$, and the many nonprompt π's guarantee this.

(b) $Bq \to B^*q$. Either the baryon system B^* or the quark may be the jet. The entire octet and decouplet, $N(B^*) = 8 + (2)10 = 28$, can contribute. Allowing another 25% from still higher baryon states gives the estimate $N(B^*) \sim 35$ and

$$E\frac{d\sigma}{d^3p}(pp \to jet(\text{baryon induced})) \simeq 70E\frac{d\sigma}{d^3p}(pp \to p(\text{prompt})) \simeq 56E\frac{d\sigma}{d^3p}(pp \to p(\text{total})), \quad (10.2)$$

where we again employ an estimated prompt/total ratio of 0.8.

Combining (a) and (b) we have

$$E\frac{d\sigma^{\text{CIM}}}{d^3p}(pp \to \text{jet}) = 27\left(8\epsilon^9 p_T^{-8}\right) + 56\left(500\epsilon^7 p_T^{-12}\right). \quad (10.3)$$

The numbers in parentheses are the $pp \to \pi$ and $pp \to p$ large-p_T single-particle cross sections. The contribution of the direct processes for baryon production and the $M\bar{M} \to q\bar{q}$ subprocesses are relatively small.

Comparing these results with the $p_T^{-4}\epsilon^7$ jet cross section, Eq. (9.5), arising from q-q scattering, we see that the CIM terms are dominant until $p_T \simeq 4.6$ (6.5) GeV/c for $\alpha_s = 0.3$ (0.15).

Including both the CIM and $qq \to qq$ contributions, the total jet/measured single-pion cross section is predicted to be

$$R = 27 + \frac{3500}{\epsilon^2 p_T^4} + \frac{0.3\alpha_s^2 p_T^4}{\epsilon^2}, \quad (10.4)$$

where we have taken $Ed\sigma/d^3p(pp \to \pi X) = 8\epsilon^9/p_T^8$ for the π^+, π^- average. For $\sqrt{s} = 23.7$ GeV ($p_{\text{lab}} = 300$ GeV/c) and $\alpha_s = 0.3$, this gives $R = 62$, 55, and 172 at $p_T = 3$, 4, and 6 GeV/c, respectively. Thus we expect a jet/single ratio greater than 50 and increasing rapidly at higher p_T values. The ultimate ratio at large p_T—once the $qq \to qq$ scattering contribution dominates the single-particle cross section—is $R = 72\epsilon^{-2}$. The last term can be further enhanced by gluon-quark and gluon-gluon interactions which have been estimated in Ref. 8.[27]

XI. DISCUSSION

The analytic results, Eqs. (9.7) and (3.18), for general reactions $A + B \to C + X$ are extremely useful, not only for high-p_T reactions, but also for calculations in other contexts, e.g., the two photon processes $e^-e^- \to e^-e^-$ $e^-e^- \to e^-e^-\gamma\gamma \to e^-e^-CX$, and single lepton production in hadron collisions. The results are a realization of the dimensional- and spectator-counting rules at large p_T and large θ_{cm}:

$$E\frac{d\sigma}{d^3p} = \sum_{\text{subprocesses}} (p_T^2+M^2)^{2-n_{\text{active}}} F(\epsilon, \theta_{\text{cm}})$$

$$\epsilon \simeq 0 \sum (p_T^2+M^2)^{2-n_{\text{active}}} \epsilon^F g(\theta_{\text{cm}}), \qquad (11.1)$$

where $\epsilon = 1 - x_R = \mathfrak{M}^2/s$. Here n_{active} is the number of active fields in the high-p_T subprocess (e.g., $n_{\text{active}}=4$ for $qq \to qq$, 6 for $qM \to qM$, 8 for $qB \to qB$) and $F = 2n_{\text{spect}} - 1$ where $n_{\text{spect}} = n(\bar{a}A) + n(\bar{b}B) + n(\bar{C}c)$ is the minimum number of elementary constituents required in the fragmentations $A \to a$, $B \to b$, $c \to C$ (e.g., $n_{\text{spec}} = 5$ and $F = 9$ for $qq \to qq$ or $qM \to qM$ in $pp \to MX$).

The spectator-counting prediction for $G_{a/A}(x)$ at $x \to 1$ is $G_{a/A}(x) \propto (1-x)^{2n(\bar{a}A)-1}$ where $n(\bar{a}A)$ is the number of fast elementary constituents of the bound state A which are left behind after fragmentation. Examples are $\nu W_{2p} \sim G_{q/B} \sim (1-x)^3$, $G_{M/B} \sim (1-x)^5$, $G_{q/M} \sim (1-x)^1$. These predictions are again based on the short-distance behavior of lowest-order terms in renormalizable perturbation theories assuming a finite Bethe-Salpeter wave function at the origin. [In cases where a is a fermion and A is a boson (or vice versa) the power can be increased by 1 from spin effects, although this effect is generally canceled by nonleading corrections. In the case of elementary bremsstrahlung in perturbation theory one has $G_{\gamma/e}(x) \sim \alpha/\pi \ln (s/m^2)[1+(1-x)^2]/x$ etc., where the logarithm arises from the $\vec{k}_T$ integration.]

In general, one predicts that aside from normalization effects the subprocesses with the minimum n_{active} (minimum p_T^{-1} power) will dominate the cross section at large p_T and small ϵ. Thus, given the fact that the $qq \to qq$ term has a small predicted normalization as shown in Sec. VI, the dominant terms (for $p_T \lesssim 7$ GeV) for $pp \to \pi^{\pm}, K^{\pm}X$ will come from the $qM \to qM$ subprocess [Fig. 7(a)]:

$$E\frac{d\sigma}{d^3p}(pp \to \pi^{\pm,0}, K^{\pm}X) \sim I\epsilon^9 (p_T^2+M^2)^{-4} f(\theta). \qquad (11.2)$$

Here M^2 represents terms of order $\langle \vec{k}_T^2 \rangle$, m_q^2, etc. All other quark-hadron subprocesses lead to a higher power of $1/p_T$ or ϵ. In the case of K^- production, the dominant contribution at high p_T and very small ϵ will come from the "fusion" subprocess $q\bar{q} \to K^- M$ [Fig. 7(b)]

$$E\frac{d\sigma}{d^3p} = I\epsilon^{11} (p_T^2+M^2)^{-4} f(\theta),$$

whereas at moderate ϵ, the $qM \to qM$ ϵ^{13} terms discussed in the text, Eq. (6.4), will dominate. A comparison of the CIM predictions with the experimentalists' fits to the Chicago-Princeton (CP) data[1] for $pp \to \pi^{\pm}, K^{\pm}, pX$ is shown in Table IV. The agreement is very good. For example, as shown in Fig. 14, the best fit quoted for the $\theta_{\text{cm}} = 90°$ data for $pp \to \pi^+ X$ is $p_T^{-8.2}(1-x_T)^{9.0}$ (with uncertainties in n and F order ± 0.5). The relative decrease of the π^-/π^+ ratio from ~unity as x_T increases evidently reflects the relative suppression of the d/u quark ratio in the proton structure function at large x as remarked in Sec. VI.

TABLE IV. Scaling predictions for $Ed\sigma/d^3p = Cp_T^{-n}(1-x_T)^F$.

Large-p_T process	Leading CIM subprocess	Predicted $n;F$	Observed (CP)[a] $n;F$
$pp \to \pi^+ X$	$qM \to q\pi^+$	8;9	8.2;9.0
π^-	$qM \to q\pi^-$	8;9	8.5;9.9
K^+	$qM \to qK^+$	8;9	8.4;8.8
K^-	$q\bar{q} \to MK^-$	8;11	8.9;11.7
	$qM \to qK^-$	8;13	
$pp \to pX$	$qB \to qp$	12;7	11.7;6.8
$pp \to \bar{p}X$	$q\bar{q} \to B\bar{p}$	12;11	(8.8;14.2)
	$qB \to q\bar{p}$	12;15	
$\pi p \to \pi X$	$qM \to q\pi$	8;7	
	$\pi q \to \pi q$	8;3	
	$q\bar{q} \to M\pi$	8;5	

[a] Reference 1.

An important check on the identification of the underlying subprocesses is the angular dependence of its cross section. The leading CIM contribution to $pp \to \pi^+ X$ arises from $u\pi^+ \to u\pi^+$:

$$\frac{d\sigma}{d\hat{t}}(u\pi^+ \to u\pi^+) = \frac{\pi\alpha_M^2}{\hat{s}^4}\left(\frac{2}{1+z}\right)^3. \qquad (11.3)$$

The angular dependence of the subprocess can be determined from experiment either from the correlated angular dependence of the away-side jet[28] or the angular dependence of the $pp \to \pi X$ inclusive cross sections.[9] Both analyses indicate that the

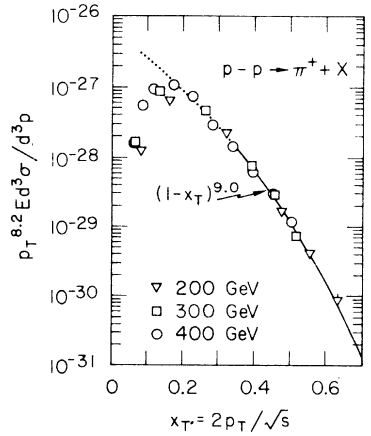

FIG. 14. Scaling-law fit to the cross section $pp \to \pi^+ X$, $\theta_{\text{c.m.}} \cong 90°$, $x_T = 2p_T/\sqrt{s} > 0.3$. From Ref. 1.

data are best fitted with the form

$$\frac{d\sigma}{d\hat{t}} \propto \frac{1}{\hat{s}\hat{t}^3} \text{ or } \frac{1}{\hat{s}\hat{u}^3}$$

(equivalent because of the $p\bar{p}$ symmetry). This coincides with the CIM *prediction* [Eq. (11.3)] for the angular dependence reflecting elementary spin-$\frac{1}{2}$ exchange. It should be emphasized, though, that phenomenological analyses which use the opposite-side jet distribution can be complicated by spectator effects unless the particles in the jet are required to have a sufficiently large p_T.

Since the values of the basic quark-hadron couplings α_M and α_B are determined by exclusive processes, predictions of the CIM for inclusive reactions are almost completely constrained: The model predicts the p_T power, $(1-x_R)$ power, and angular shape, as well as the normalization for each contributing subprocess. As an example, for $K^+(\pi^+)$ production in proton-proton collision the dominant CIM subprocess is $uK^+ \to uK^+$ which contributes (in GeV units) using [Eq. (6.1)]

$$E\frac{d\sigma}{d^3p}(pp \to K^+X) \sim 3\frac{\epsilon^9}{p_T^8}\left[1 + x_R z)^{-5} + (1 - x_R z)^{-5}\right]. \tag{11.4}$$

This estimate has theoretical uncertainties of a factor of 2. This can be compared to the fit to the CP data[1] at 90°,

$$Ed\sigma/d^3p(pp \to K^+X) \sim 5(1 - x_T)^{8.4\pm0.5}/p_T^{8.8\pm0.5}.$$

Thus the normalization of the $qM \to qM$ amplitude as determined from exclusive reactions and form factors is of the correct size to account for the Fermilab data. The prediction for π^+ is similar but somewhat higher due to the larger number of decay channels and to possible SU(3)-breaking effects.

The leading CIM contribution to K^- production at very large x_T is expected to be due to the "fusion" subprocesses $q\bar{q} \to M\bar{M}$. For K^- production this includes $u\bar{u} \to K^+K^-$, $d\bar{u} \to K^0K^-$ as well as K^* contributions. Specifically, at 90° the yield for $pp \to K^-X$ is

$$0.02\frac{\epsilon^{11}}{p_T^8} \tag{11.5}$$

for the contribution of the *single subprocess* $u\bar{u} \to K^+K^-$ alone. The calculation includes a factor of $\frac{1}{3}$ from the fact that quarks of the same color must annihilate and $\frac{1}{2}$ from the spin crossing factor. This is useful for an estimate of how often a K^- trigger will be balanced on the away side by exactly one particle, the K^+, in the CIM. Taking all the prompt fusion contributions, the coefficient in Eq. (11.5) is increased to ~0.16. Additionally, one can expect a contribution of order $0.8(1-x_T)^{13}/p_T^8$ at 90° from $K^-u \to K^-u$ s-channel subprocesses, etc. Thus the fusion subprocesses will not dominate K^- production until $x_T \gtrsim 0.6$.

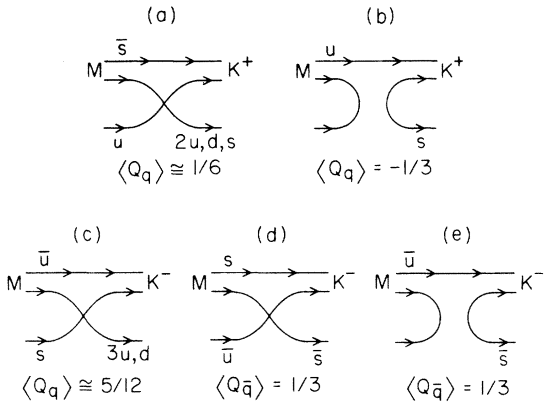

FIG. 15. Dominant CIM diagrams for $Mq \to K^{\pm}q'$ illustrating the final-state charge correlations.

The value of $\alpha_B \sim 10$ GeV^4 allowed us to predict the normalization of cross sections for baryon and antibaryon production. The leading CIM processes are $qB \to q'B'$ and $q\bar{q} \to B\bar{B}'$. The predictions are consistent with the Fermilab and ISR data as discussed in the text.

It is interesting to see how *charge correlations* between the trigger charge and the charge of fast particles on the away side arise. In the ISR domain, where x_T is small (~0.3), the dominant CIM subprocesses for $K^{\pm}$ production are $qM \to q'K$ and $qM \to q'K^* \to q'K$. The various recoil quark systems q' involved in the direct product of kaons are shown in Fig. 15. (Notice that the strange meson M in Fig. 15(a) is found in proton Fock-state components with ≥ 5 quarks, and the recoil quark has a roughly equal chance [assuming SU(3) symmetry] to be an s or d or either of the two u quarks.) As shown in Fig. 15, the quark system opposite the trigger is always positively charged for a K^-, and roughly neutral (or slightly positive) for the K^+. [The s-pole contribution of Fig. 15(b) is suppressed by a factor of 2^4 at 90°.] The same results are maintained when decays of $K^* \to K\pi$ are included. In the case of the fusion contributions for K^-, the recoil system tends to have charge 0 or +1, so again the K^- tends to be balanced by positive charge. The charge correlations for p and $\bar{p}$ are predicted to be similar to those for K^+ and K^- triggers, respectively.

Since the CIM processes always involve flavored-quark exchange, charge correlations between the trigger and away-side systems occur naturally. In contrast, such correlations are generally expected to be negligible for qq scattering via colored gluon exchange. It would also be interesting

to determine the charge and strangeness configurations of the spectator systems in the beam directions accompanying a particular high-p_T trigger. As emphasized elsewhere,[29] the charge flow associated with massive-lepton-pair production provides an ideal laboratory for the study of quantum-number transfer in high-energy reactions.

We have also seen in Sec. IX that contributions to single-particle production from the p_T^{-4} subprocess $qq \to qq$ are small (for $\alpha_s < 0.15$) until $p_T > 10$ GeV/c, see Eq. (9.11), due to the suppression from the effects of single-particle trigger bias. Other p_T^{-4} subprocesses, such as $gq \to gq$, $q\bar{q} \to gg$, and $gg \to gg$, are similarly suppressed.

However, there are additional processes present within the QCD framework which are not suppressed by trigger bias. At first glance the most important example is gluon + quark → meson + quark. This process yields p_T^{-6} behavior in the inclusive cross section. Using rough estimates it seems to dominate all the above mechanisms at all but the highest p_T values. However, the gauge-invariant structure of QCD leads to a remarkable cancellation among the various diagrams contributing to this process. As a result it may not play an important role in single-particle inclusive scattering, but deserves further study.

While the above p_T^{-4} processes are probably not dominant for single-particle yields until p_T is very large, measurements involving a *jet trigger* with large total transverse momentum p_T^J are important since the natural suppression of quark-quark scattering (and other processes involving gluon jets: $Mq \to gq$, $gq \to gq$, $q\bar{q} \to gg$, $gg \to gg$, etc.) due to bias from the single-particle trigger is removed.

In order to interpret such jet measurements, it is crucial to be able to distinguish the various possible contributions. This requires knowledge of the scaling behavior in p_T^J and x_T^J of the cross section and the nature of the source of the hadronic jets. At large p_T, a jet can arise from a quark, multiquark, gluon, or hadronic system. Empirical means of discriminating between them will include (1) quantum-number retention, (2) the power-law behavior in the momentum fraction x of the leading particle, and (3) the associated multiplicities.

An important theoretical and experimental question is how to define a large-p_T jet trigger which does not confuse contributions from spectator particles. In addition, the large values reported for $\langle p_T^{\text{out}} \rangle$ may indicate contributions from processes involving more than $2 \to 2$ collisions. It may be possible to resolve some of these questions by studying a "quark" jet trigger at high p_T^J in deep-inelastic lepton scattering where we "know" the subprocess is $lq \to lq$.

The cross section for $p + p \to \text{jet} + X$ with a calorimeter trigger, as defined in Ref. 30, is observed to be quite large. At $p_{\text{lab}} = 200$ GeV/c, the ratio $R = E_J d\sigma/d^3p_J(pp \to \text{jet} + X)/Ed\sigma/d^3p(pp \to \pi^* X)$ appears to be in the range 200–400 for $p_T \sim 5$ GeV. This appears to be too large to be completely accounted for by the CIM subprocesses, $Mq \to Mq$, $M\bar{M} \to q\bar{q}$, $q + qq \to M + B$, $qB \to qB$, $q\bar{q} \to M\bar{M}$. Using Eq. (10.4), for a total jet trigger one obtains a ratio R of order 50 for the above kinematics. The leading processes in the CIM scale as $E_J d\sigma/d^3p_J \sim p_T^{-8}(1 - x_{TJ})^9$.

The contribution to the jet trigger from the scale-invariant $qq \to qq$ process from Eq. (10.4) is (in GeV units)

$$E_J d\sigma/d^3p_J = 2.5\alpha_s^2(1 - x_{TJ})^7 p_{TJ}^{-4}.$$

Asymptotic-freedom-type modifications to the structure functions or quark constant can give logarithmic modifications to this result. However, it should be emphasized that the exponential factors which have been computed for gauge theories to *exclusive* quark-quark scattering *are not applicable* to inclusive reactions, since the quarks are allowed to radiate. We emphasize that any proposed scale violation from k_T fluctuations, structure functions, or quark form-factor effects must not *in total* exceed the scale violations seen in $p_T^4 Ed\sigma/d^3p(\mu p \to \mu X)$ at fixed x_T and $\theta_{\text{c.m.}}$. Double counting should be avoided.

The $qq \to qq$ contribution to the jet trigger from Eq. (10.4) for $\alpha_s = 0.3$ at $p_{\text{lab}} = 200$ GeV/c, $p_T = 5$ GeV is $R \cong 0.3\alpha_s^2 p_T^4/(1 - x_T)^2 \cong 70$. Other QCD processes involving gluons are roughly double this contribution. Thus it is possible that the CIM processes, combined with scale-invariant QCD contributions, can give jet cross sections just below the observed values. In order for this picture to be a viable and consistent explanation, however, the *jet cross* section at $p_T^J > 5$ GeV *should* begin to approach p_{TJ}^{-4} behavior at fixed x_{TJ} and $\theta_{\text{c.m.}}$

XII. CONCLUSIONS

The experimental data for single-particle and jet cross sections, charge, momentum, and angular correlations are now so extensive that the constraints on fundamental models have become overwhelmingly restrictive.

If sufficient scale breaking is assumed—either in the structure functions and/or the scattering amplitude—then it is always possible to interpret the single-particle cross sections in terms of an effective quark-quark scattering cross section. However, as we have emphasized here, it is difficult to understand the input normalizations and the strong charge correlations and momentum correlations measured by the BFS collaboration,[10] as

well as the p_T behavior for baryon production. Further, there is no obvious explanation or connection with exclusive large-p_T data.

On the other hand, the CIM, together with dimensional- and spectator-counting rules, predicts the dynamical forms and normalizations of inclusive and exclusive cross sections in terms of two fundamental coupling constants which can for instance be determined (in fact, overdetermined) from low-energy fixed-angle exclusive scattering, form-factor asymptotics, or momentum distributions. The scaling laws of the CIM assume a underlying scale-free theory (modulo logarithmic corrections) characteristic of renormalizable perturbation theories. Given that the coupling α_s of QCD is numerically small plus the strong trigger bias suppression of quark jet fragmentation, the leading subprocesses for single-particle yields then arise most naturally from quark-hadron scattering amplitudes. We emphasize that *the* $qM \to qM$, $qB \to qB$ *contributions and their crossing variants are an essential component in any model including QCD.* The calculated subprocess cross section for $\pi^{\pm}$ or K^{+} production in pp collisions is $d\sigma/dt(qM \to qM) = \pi\alpha_M^2/su^3$, where α_M is determined by the valence meson wave-function renormalization. This form then yields the observed p_T, $\theta_{\text{c.m.}}$, x_T dependence as well as the magnitude of the inclusive cross sections. However, as we have discussed in Sec. X, it does not seem possible for the quark-hadron and quark-quark processes to account for the reported large jet cross section.

As we have emphasized, processes based on quark-hadron scattering can dominate large-p_T single-particle inclusive reactions, despite their p_T^{-8}, p_T^{-12} scaling behavior, due to the absence of trigger bias and the relatively large size of α_M and α_B. The CIM terms are predicted to dominate the $qq \to qq$ scale-invariant contributions for p_T below ~7 GeV, assuming $\alpha_s = 0.3$. The crossover point in p_T^2 is controlled by the ratios α_M/α_s and $(\alpha_B/\alpha_S)^{1/2}$. For inclusive meson yields one needs an estimate of the normalization of the $G_{M/B}(x)$ structure functions for virtual $q\bar{q}$ mesonlike states. These were fixed approximately by normalizing to the measured antiquark momentum fractions. The p_T, ϵ, and angular dependence of inclusive meson and baryon production reactions can then be understood in terms of the minimal set of two subprocesses, $qM \to qM$, $qB \to qB$, and their crossing variants. The normalization of each subprocess contribution has been approximately computed. Detailed predictions for other beams (including photons and leptons) can be made using the simple general formula Eq. (3.18). There are also many important tests of the model involving correlations between particles on the same-side, away-side, and beam fragmentation regions. Occasional events are predicted to occur with a single particle in both the trigger and away-side systems, via the $q\bar{q} \to M\bar{M}$ and $q\bar{q} \to B\bar{B}$ subprocesses. These may occur at a larger rate in MB and $\bar{B}B$ collisions.

It is useful to distinguish three regions in transverse momentum for hadronic inclusive reactions at high energies:

(A) The asymptotically scale-free, large-p_T region (above $p_T \sim 7$ GeV/c for single particles, and $p_T \sim 5$ GeV/c for jets), where the simple perturbation-theory contributions for QCD are expected to dominate if $\alpha_s \cong 0.3$. In this region, in which strong interactions take their most elementary form, one will be able to study the properties of quark and gluon jets, as well as multiquark jets in the spectator regions.

(B) The moderate-p_T zone, where the CIM diagrams are predicted to dominate giving scaling law contributions of the form $p_T^{-8}, p_T^{-12} \cdots$ at fixed x_T, depending on the detected particle. In this region (roughly $2 < p_T < 7$ GeV/c for single-particle reactions), one can trace the quantum-number flow characteristic of duality diagrams. Thus, the dynamical structure of hadron wave functions can be studied in detail in this region. In the case of exclusive reactions, Regge behavior takes its most basic form, with trajectories $\alpha(t)$ receding to negative integers, or in the case of Compton scatter-in to a $J = 0$ fixed pole.

(C) The most complicated region is at low p_T where the cross sections Feynman-scale and many different coherent, diffractive, Regge, and resonance/cluster phenomena operate. In the central rapidity regions correlations with the quantum numbers of the incident particles become negligible, but the multiplicity in the central region may well be related to the same color confinement dynamics in the $e^+e^- \to$ hadrons. Furthermore, the fragmentation regions with $x_L = p_L^{\text{cm}}/p_L^{\max} \to \pm 1$ can also be related to off-shell hadron dynamics, and spectator quark counting rules can be used to discriminate the basic hadronic mechanics at low transverse momentum.

The transition regions between (A) and (B) or (B) and (C) are clearly complicated since several different mechanisms compete, but phenomena in such regions could be important for the study of interference effects, etc. Photon/hadron comparisons are especially important; in regions (A) we predict $\gamma/\pi \sim$ const. at fixed x_T; in region (B) $\gamma/\pi \sim \alpha p_T^2$.

We note that in the CIM several different areas of hadron phenomenology become interconnected: (a) form factors, (b) large t and u exclusive reactions, (c) Regge behavior at large t, (d) particle yields for x_L near ± 1 at low t, and (e) large-p_T inclusive reactions. The model satisfies the corres-

pondence principle, in the sense of Bjorken and Kogut,[25] and provides a smooth connection between these various regions and phenomena.

We have tried to show in this paper that the normalization of the various CIM contributions to inclusive scattering are fixed by external constraints and are not arbitrary. They are of a reasonable size to explain the moderate-transverse-momentum single-particle yields ($p_T < 7$ GeV/c) and qualitative features of the charge correlations. *The* CIM *is consistent with* QCD, for example, whereas *arbitrarily omitting the* CIM *diagrams would not be internally consistent.* The CIM calculational rules, however, do not explicitly include any logarithmic variations which are expected in such asymptotically free theories (mostly for reasons of simplicity).

We thus see that a theory of short-distance hadronic processes patterned after asymptotically free QCD is tenable. CIM processes based on quark-hadron scattering are required for theoretical completeness and describe the experimental data at intermediate p_T. Quark-quark scattering and related processes involving gluons will dominate at high values of p_T; the precise crossover point depends on the value of α_s. Thus a rather complete model of short-distance processes exists which is consistent with a fundamental quark-quark interaction, in particular QCD, and which enjoys considerable phenomenological success.

ACKNOWLEDGMENTS

We wish to thank our colleagues, particularly J. Bjorken, W. Caswell, T. DeGrand, and R. Horgan for helpful discussions. We also wish to thank D. Jones for checking many of the calculations. This work was supported in part by the Department of Energy. One of us (J. F. G.) is an A. P. Sloan Foundation Fellow.

APPENDIX A: ACCURACY OF GENERAL FORMULA (3.18)

The hard-scattering formula for processes not involving final-state fragmentation (applicable to CIM prompt processes and also quark or gluon jet cross sections) can be written in the form[7]

$$E\frac{d\sigma}{d^3p}(A+B\to C+D)=\frac{2}{\pi}\sum_{ab}\int_{-(1-2x_2)}^{(1-2x_2)}\frac{dz}{1-z^2}F_{a/A}\left(\frac{2x_1}{1+z}\right)F_{b/B}\left(\frac{2x_2}{1-z}\right)\frac{d\hat{\sigma}}{dt}\left(\hat{s}=\frac{4p_T^2}{1-z^2},z\right)\Bigg|_{ab\to Cd}, \tag{A1}$$

where $F(x)=xG(x)$, and the integration variable z is the cosine of the scattering angle in the subprocess center of mass. The overall kinematics is specified by $x_1=-u/s$, $x_2=-t/s$, and p_T^2, with $\epsilon=1-x_R=1-x_1-x_2$ [(see Eq. (3.14)]. The leading behavior at large p_T and $\epsilon\to 0$ is given by Eq. (3.18). To illustrate the accuracy of this latter form, we compare the two formulas for the case of the $qM\to qM$ (ut) subprocess contribution to $pp\to MX$. Here $d\hat{\sigma}/dt=\pi\alpha_M^2/\hat{s}\hat{u}^3$, and we take $F_{M/p}(x)=6(1-x)^5$ for $x>0.3$, $F_{q/p}(x)=4(1-x)^3$ for $x>0.2$, and constant otherwise, as in Eq. (3.1). For pion beams, we use $F_{M/\pi}(x)=4(1-x)^3$ for $x>0.4$ as in Table II.

Equation (3.18) then gives for $\theta_{\text{c.m.}}=90^\circ$:

$$E\frac{d\sigma}{d^3p}(pp\to MX)=\frac{2^5}{21}\alpha_M^2\frac{(1-x_T)^9}{p_T^8}. \tag{A2}$$

In Table V we show the ratio of (A1) to (A2) [the quantity defined as $J(x_T)$ in Eq. (3.18)] as a function of x_T at 90°, and also the effective power F_{eff} of $\epsilon=(1-x_T)$ obtained for $p_T^8 Ed\sigma/d^3p$ from (A1). We see that for $x_T>0.3$, the simple form (A2) is accurate in normalization to within 25%. Furthermore, we see that the power behavior $(1-x_T)^9$ predicted by the spectator counting rule ($F=2n_{\text{spect}}-1$) is accurate to within $\sim\frac{1}{2}$ units for $x_T>0.4$, and the effective F power decreases below this point.[31]

TABLE V. Accuracy of general formula (3.18).

x_T	$J(pp\to M)$	$F_{\text{eff}}(pp)$	$J(\pi p\to M)$	$F_{\text{eff}}(\pi p)$	$[F(pp)-F(\pi p)]_{\text{eff}}$
0.1	0.37	3.8	0.42	3.8	0
0.2	0.63	5.0	0.58	4.5	0.5
0.3	0.99	6.3	0.77	5.0	1.3
0.4	1.23	8.6	1.00	5.6	3.0
0.5	1.19	9.3	1.14	6.9	2.4
0.6	1.13	9.2	1.10	7.2	2.0
0.7	1.09	9.1	1.05	7.1	2.0
0.8	1.05	9.0	1.02	7.0	2.0
0.9	1.02	9.0	1.01	7.0	2.0

It should be emphasized that the effective power $F_{\rm eff}$ is in general expected to decrease in regions where the structure functions $F(x)$ are flat, i.e., for $x_T < \min(x_a, x_b)$. Thus, a fit to $F_{\rm eff}$ over the region $0.2 < x_T < 0.4$ for the above example should give a value of $\overline{F}_{\rm eff} \sim 6$ for $pp \to M$ and $\overline{F}_{\rm eff} \sim 5$ for $\pi p \to M$, yielding a ratio that varies as $\Delta F_{\rm eff} \sim 1$. On the other hand, for $x_T > 0.6$, $\Delta F_{\rm eff}$ equals 2 to high accuracy in agreement with the spectator-counting rules.

APPENDIX B: COUPLING-CONSTANT CONSISTENCY

In Secs. III, IV, and V we have shown that the values $\alpha_M \sim 2$ GeV^2 and $\alpha_s \sim 10$ GeV^4 for the meson $q\bar{q}$ and baryon qqq couplings are consistent with the normalization of large-angle elastic reactions and the momentum distribution functions. We demonstrate here that a similar consistency is present when comparing the above determinations to that obtained from the asymptotic behavior of meson and baryon form factors at large t. We also define here the relationship of α_M and α_B to the Bethe-Salpeter wave function.

Let us consider the q-$\bar{q}$ Bethe-Salpeter wave function $\Psi(p,k)$ for the bound-state pseudoscalar meson: We define

$$\Psi(p,k) = (m + \tfrac{1}{2}\not{p} - \not{k})\gamma_5 \psi(k)(m - \tfrac{1}{2}\not{p} - \not{k}) , \qquad \text{(B1)}$$

where $\psi(k)$ is the usual amputated vertex function, $\phi(k)$, divided by the propagators

$$[(p/2 - k)^2 - m^2][(p/2 + k)^2 - m^2] .$$

The calculation of high-p_T processes require knowledge of $\Psi(p,l)$ at large relative momentum l. One can iterate the Bethe-Salpeter equation once and obtain

$$\Psi(p,l) = (m + \tfrac{1}{2}\not{p} - \not{l})^{-1} \times \int \frac{d^4k}{(2\pi)^4 i} V(l-k)\Psi(p,k)(m - \tfrac{1}{2}\not{p} - \not{l})^{-1} \qquad \text{(B2)}$$

In the case of single gluon exchange, for large l we can approximate $V(l-k) \sim V(l) \sim \gamma_\alpha^a g_s^2 \gamma_b^\alpha / l^2$. Furthermore, in the region of integration where k is small, we can drop the k dependence in the Dirac numerator of the equation for $\Psi(p,k)$, thereby obtaining at large relative momentum

$$\Psi(p,l) \simeq (m + \tfrac{1}{2}\not{p} - \not{l})^{-1} \frac{g_s^2}{l^2} \gamma_\alpha (\tfrac{1}{2}\not{p} + m) \times \gamma_5 \gamma^\alpha \tilde{\psi}(0)(m - \tfrac{1}{2}\not{p} - \not{l})^{-1} . \qquad \text{(B3)}$$

The quantity

$$\tilde{\psi}(0) = 2m \int \frac{d^4k}{(2\pi)^4 i} \psi(k) \qquad \text{(B4)}$$

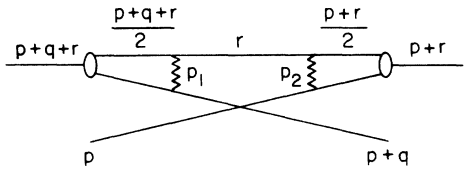

FIG. 16. Diagram for quark-meson scattering using the iteration of the gluon-exchange kernel in both Bethe-Salpeter wave functions.

can be directly identified with the nonrelativistic wave function at the origin. The approximations are justified as long as the integration over k^μ converges. In asymptotic-freedom theories, one obtains a mild logarithmic divergence[11] which can reflect itself in corresponding logarithmic modifications to the final scaling laws.

We can now calculate the quark-meson scattering amplitude of Fig. 16 at large momentum transfer. For a quark of one specific color we have

$$\mathfrak{M} = \bar{u}(p+q)\gamma_\alpha [m_q + \tfrac{1}{2}(\not{p} + \not{q} + \not{r})]\gamma_5 \gamma^\alpha \not{r} \times \gamma_\beta [m_q + \tfrac{1}{2}(\not{p} + \not{r})]\gamma_5 \gamma^\beta u(p) \times \tilde{\psi}^2(0) g_s^4 (r^2 p_1^2 p_2^2)^{-1} C , \qquad \text{(B5)}$$

where C is a color factor to be defined shortly. The spin-averaged square of the matrix element for $|t|, |u| \gg m^2$ is

$$\tfrac{1}{2} \sum_{\rm spins} |\mathfrak{M}|^2 = 16 \frac{s}{u^2} (g_s^2)^4 C^2 \tilde{\psi}^4(0) . \qquad \text{(B6)}$$

The color factor per average color quark in SU(n) is

$$C = \frac{1}{n}\frac{1}{4}\frac{(n^2-1)^2}{n} = \frac{16}{9} \ (\text{for } n = 3) , \qquad \text{(B7)}$$

where our normalization is conventional (see the text, Sec. IX). Thus

$$\frac{d\sigma}{dt} = \frac{1}{16\pi s^2}\frac{1}{2}\sum_{\rm spins} |\mathfrak{M}|^2 = \frac{C^2}{\pi}\frac{1}{su^3}[g_s^2 \tilde{\psi}(0)]^4 \equiv \pi \left(\frac{1}{3}\frac{g^2}{4\pi}\right)^2 \frac{1}{su^3} . \qquad \text{(B8)}$$

We can now identify

$$\alpha_M \equiv \frac{1}{3}\frac{g^2}{4\pi} = \frac{16}{9\pi}[g_s^2 \tilde{\psi}(0)]^2 , \qquad \text{(B10)}$$

i.e., the dimensional coupling constant g is

$$g = 4 g_s^2 \tilde{\psi}(0)(4/3)^{1/2} .$$

Let us now turn to the form-factor calculation. In a naive approach one is tempted to obtain the asymptotic behavior at large t from the graphs in

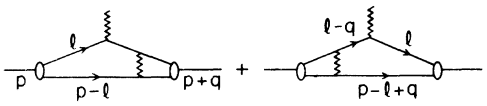

FIG. 17. Diagrams for meson form factor at large momentum transfer in which only one wave function is iterated.

which only one wave function is iterated (see Fig. 17). However, the x-integration in the d^4l loop (x is the light-cone fraction of momentum carried by the quark struck by the photon) then becomes singular at $x \to 1$,

$$\sim \int^{1-M^2/q^2} \frac{dx}{1-x},$$

and extreme values of the quark momenta are probed. The wave-function approximation is thus not applicable for the main loop integration over l. Accordingly, we must iterate the Bethe-Salpeter kernel once more and calculate the graph of Fig. 18.[22] We shall use the general Lorentz frame (P is arbitrary) (see, e.g., Appendix B, Ref. 7)

$$\begin{aligned} p &= \left(P+\frac{M^2}{4P}, \vec{0}_T, P-\frac{M^2}{4P}\right), \\ p-l &= \left((1-x)P+\frac{m^2+\vec{l}_T^{\,2}}{4(1-x)P}, -\vec{l}_T, (1-x)P \right. \\ &\qquad \left. -\frac{m^2+\vec{l}_T^{\,2}}{4(1-x)P}\right), \\ q &= \left(\frac{\vec{q}_T^{\,2}}{4P}, \vec{q}_T, -\frac{\vec{q}_T^{\,2}}{4P}\right), \end{aligned} \tag{B11}$$

where $q^2 = -\vec{q}_T^{\,2}$, and $x = (l_0+l_3)/(p_0+p_3)$ is the usual light-cone/infinite-momentum fraction carried by the struck quark. The matrix element is

$$\begin{aligned} \mathfrak{M}_\mu = \int \frac{d^4l}{(2\pi)^4 i} \mathrm{Tr}[&(m+\tfrac{1}{2}\not{p}+\not{q})\gamma^\alpha(m+\not{l}+\not{q})\gamma_\mu(m+\not{l})\gamma^\beta \\ &\times (m+\tfrac{1}{2}\not{p})\gamma_\beta(m-\not{p}+\not{l})\gamma_\alpha][\tilde{\psi}(0)\, g_s^{\,2}]^2 \\ &\times [l^2(p-l)^2(l+q)^2 p_1^{\,2} p_2^{\,2}]^{-1} C'. \end{aligned} \tag{B12}$$

Here the color factor is $C' = \frac{16}{3}$ (we sum over colors for the form factor). Using standard techniques—i.e., picking up the $(p-l)^2$ pole where $p_1^{\,2} \cong \frac{1}{2}l^2$, $p_2^{\,2} \cong \frac{1}{2}(l+q)^2$—the above integral reduces to

$$\frac{16}{3}\int_0^1 \frac{dx}{2(1-x)} \int \frac{d^2l_t}{(2\pi)^3} \frac{[\tilde{\psi}(0) g_s^{\,2}]^2 \mathrm{Tr}[\cdots]}{D},$$

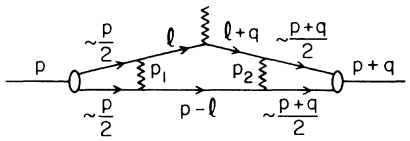

FIG. 18. Diagram for meson form factor using the iternation of the gluon exchange kernel in both Bethe-Salpeter kernels.

where

$$\begin{aligned} D = {} & \tfrac{1}{4}(1-x)^{-4}[\vec{l}_T^{\,2}+M^2(x)]^2 \\ & \times\{[\vec{l}_T^{\,2}+(1-x)\vec{q}_T]^2+M^2(x)\}^2 \end{aligned}$$

and

$$M^2(x) \equiv m_q^{\,2} - x(1-x)M^2. \tag{B13}$$

The trace reduces at large $q^2 = -\vec{q}_T^{\,2} = t$:

$$\mathrm{Tr}[\cdots] = \tilde{M}^2(x)x(1-x)^2 4tp_\mu, \tag{B14}$$

where $\tilde{M}^2(x)$ is a complicated combination of quark and meson masses. There are two important regions of the $\vec{l}_T$ integration—$\vec{l}_T \sim 0$ and $\vec{l}_T \sim -\vec{q}_T(1-x)$, providing an extra factor of 2. Writing $\mathfrak{M}_\mu = F(t)(2p_\mu + q_\mu)$ we obtain at large t

$$\begin{aligned} F(t) &\sim \frac{16}{3}\int_0^1 \frac{dx}{2(1-x)} \int \frac{\pi dl_T^{\,2}}{(2\pi)^3} \frac{[g_s^{\,2}\tilde{\psi}(0)]^2 4x(1-x)^2 t\tilde{M}^2(x)}{\frac{1}{4}[l_T^{\,2}+M^2(x)]^2 t^2} \\ &\sim \frac{1}{t}\left\langle\frac{\tilde{M}^2(x)}{M^2(x)}\right\rangle \frac{8}{9\pi^2}[g_s^{\,2}\tilde{\psi}(0)]^2 \end{aligned} \tag{B15}$$

Substituting in terms of g^2, or rather α_M, we have

$$tF(t) \sim \frac{\alpha_M}{2\pi}\left\langle\frac{\tilde{M}^2(x)}{M^2(x)}\right\rangle. \tag{B16}$$

Since $\tilde{M}^2(x) \sim M^2(x)$, it is clear that the coefficient of $1/t$ is of order 0.25–1.0 GeV^2 if $\alpha_M = 2$ GeV^2. In a monopole fit to data, one has

$$tF(t) \sim M^2 \sim 0.5\ (\mathrm{GeV})^2.$$

Clearly, the agreement is acceptable.

In the baryon case where $\alpha_B = 10$, one similarly can show that the asymptotic behavior of the proton form factor is also satisfactorily normalized. The larger value of α_B, compared to α_M, is required, in part, in order to compensate the more strongly damped x integral in the baryon case. One finds $\alpha_B \int dx\, x(1-x)^3$ vs $\alpha_M \int dx\, x(1-x)$ in the baryon-meson cases, respectively.

[1]J. W. Cronin *et al.*, Phys. Rev. D 11, 3105 (1975); D. Antreasyan *et al.*, Phys. Rev. Lett. 38, 112 (1977).

[2]G. Donaldson *et al.*, Phys. Rev. Lett. 36, 1110 (1976). See also E. Malamud, in Proceedings of the VIII International Symposium on Multiparticle Dynamics, Kaysersberg, 1977 (unpublished).

[3]F. W. Büsser *et al.*, Nucl. Phys. B106, 1 (1976).

[4]B. Alper *et al.*, Nucl. Phys. B100, 237 (1975).

[5]S. M. Berman and M. Jacob, Phys. Rev. Lett. 25, 1683 (1970); S. M. Berman, J. D. Bjorken, and J. B. Kogut, Phys. Rev. D 4, 3388 (1971); J. Bjorken *ibid.* 3098 (1973). See also R. F. Cahalan, K. A. Geer, J. Kogut, and L. Susskind, *ibid.* 11, 1199 (1975); M. Bander, M. Barnett, and D. Silverman, Phys. Lett. 48B, 243 (1974).

[6]R. Blankenbecler, S. J. Brodsky, and J. F. Gunion, Phys. Lett. B39, 649 (1972); 42, 461 (1973); Phys. Rev. D 12, 3469 (1975). Spectator-counting rules for structure functions are derived in R. Blankenbecler and S. J. Brodsky, *ibid.* 10, 2973 (1974); J. Gunion, *ibid.* 10, 242 (1974). The fusion reactions $q\bar{q} \to M\bar{M}$ have been particularly emphasized by P. V. Landshoff and J. C. Polkinghorne, *ibid.* 10, 891 (1974). See also M. K. Chase and W. J. Stirling, Nucl. Phys. B133, 157 (1978), and references therein.

[7]For a general review, see D. Sivers, S. J. Brodsky, and R. Blankenbecler, Phys. Rep. 23C, No. 1 (1976). See also Refs. 13, 15, and S. J. Brodsky, R. Blankenbecler, and J. F. Gunion, in *Leptons and Multileptons*, proceedings of the XII Rencontre de Moriond, Flaine, France, edited by J. Trân Thanh Vân (Editions Frontières, Paris, 1977). Our values for $\pi^{\pm}p \to \pi^{\pm}p$ are from the recent measurements of K. A. Jenkins *et al.*, Phys. Rev. Lett. 40, 425 (1978).

[8]For models with strong scale violation (power-law breaking of scaling) of the structure functions see E. Fischbach and G. W. Look, Purdue University report, 1977 (unpublished); A. P. Contogouris, R. Gaskell, and A. Nicolaidis, McGill report, 1978 (unpublished); R. Hwa, A. J. Speissbach, and M. J. Teper, Phys. Rev. Lett. 36, 1418 (1976). For models using conventional QCD scale breaking see D. Sivers and R. Cutler, Phys. Rev. D 16, 679 (1977) and B. Combridge, J. Kripfganz, and J. Ranft, Phys. Lett. 70B, 234 (1977); A. P. Contogouris, R. Gaskell, and S. Papadopoulos, McGill report, 1978 (unpublished); J. F. Owens, E. Reya, and M. Glück, Phys. Rev. D (to be published). See also F. Hulzen, G. A. Ringland, and R. G. Roberts, Phys. Rev. Lett. 40, 991 (1978); R. Raitio and R. Sosnowski, Helsinki University Report No. TFT-77-29, 1977 (unpublished); M. Chase, DAMTP Report No. 77/29 (unpublished); R. D. Field, CalTech report, 1978 (unpublished).

[9]R. D. Field and R. P. Feynman, Phys. Rev. D 15, 2590 (1977); R. P. Feynman, R. D. Field, and G. C. Fox, Nucl. Phys. B128, 1 (1977); G. C. Fox, in *Particles and Fields '76*, proceedings of the Annual Meeting of the Division of Particles and Fields of the APS, edited by H. Gordon and R. F. Peierls (BNL, Upton, New York, 1977), p. 61.

[10]R. Møller, in *Leptons and Multileptons*, proceedings of the XII Rencontre de Moriond, Flaine, France, edited by J. Trân Thanh Vân (Editions Frontières, Paris, 1977); G. Böggild, in Proceedings of the VIII International Symposium on Multiparticle Dynamics, Kayserberg, France, 1977 (unpublished). We note that such charge correlations might be explained if $q\bar{q} \to q\bar{q}$ or $gg \to q\bar{q}$ annihilation subprocesses play a dominant role. However, calculations in the framework of QCD, as well as crossing symmetry arguments, predict that such contributions are unimportant.

[11]The relatively small amount of scale breaking seen in the lepton-pair production continuum cross section and recent deep-inelastic neutrino cross sections suggests that such effects probably introduce only logarithmic changes to the large p_T scaling laws. Logarithmic corrections to exclusive dimensional counting rules in an asymptotic-freedom theory are discussed by T. Appelquist and E. Poggio, Phys. Rev. D 10, 3280 (1974).

[12]P. Darriulat, in *Proceedings of the XVIII International Conference on High Energy Physics, Tbilisi, 1976*, edited by N. N. Bogolubov *et al.* (JINR, Dubna, U.S.S.R., 1977). See also C. Escobar, Phys. Rev. D 15, 355 (1977).

[13]P. Darriulat *et al.*, Nucl. Phys. B107, 429 (1976).

[14]S. D. Ellis, M. Jacob, and P. V. Landshoff, Nucl. Phys. B108, 93 (1976); M. Jacob and P. Landshoff, *ibid.* B113, 395 (1976); J. D. Bjorken and G. R. Farrar, Phys. Rev. D 9, 1449 (1974). The BFS data, Ref. 10, indicate pion-trigger contributions from K^0, K^*, ρ^0, Δ, and N^* decays. The estimate for resonances of Ellis *et al.* which focused on ρ-decay contributions alone gave a lower prompt ratio for pions. Note that Eq. (6.2) favors a value of $f_p \sim \frac{1}{2}$, which is consistent with our analysis if $\langle x_E^{\max} \rangle \sim 1.07$.

[15](a) See M. Della Negra, in Proceedings of the VII International Colloquium on Multiparticle Reactions, Tutzing, 1976 (unpublished) and references therein. (b) For a recent analysis of the neutron and proton structure functions, see Ref. 26. Notice that $f_{u/p} < 2f_{d/p}$ since the sea-quark contributions tend to neutralize flavor differences. A more accurate treatment of the valence contributions with $G^V_{u/p} \gg G^V_{d/p}$ at $x \to 1$ is required for the analysis of $\pi^{\pm}$ differences.

[16]S. J. Brodsky and G. Farrar, Phys. Rev. Lett. 31, 1153 (1973); Phys. Rev. D 11, 1309 (1975); V. Matveev, R. Muradyan, and A. Tavkhelidze, Lett. Nuovo Cimento 7, 719 (1973). For a discussion of applications to nuclear systems see R. Blankenbecler, in Proceedings of the VIII International Symposium on Multiparticle Dynamics, Kaysersberg, 1977 (unpublished), and S. Brodsky and B. Chertok, Phys. Rev. 14, 3003 (1976); Phys. Rev. Lett. 37, 269 (1976).

[17]There are also important terms (diquark exchange) which have $\alpha(t) \to -2$. For a general discussion of the connection between Regge and power-law fixed-angle behavior see R. Blankenbecler, S. J. Brodsky, J. F. Gunion, and R. Savit, Phys. Rev. D 8, 4117 (1973); D. D. Coon, J. F. Gunion, J. Trân Thanh Vân, and R. Blankenbecler, Phys. Rev. D (to be published). G. Grunberg, Phys. Rev. D 16, 646 (1977). For other discussions of the angular distributions from quark exchange, see also T. Uematsu, Prog. Theor. Phys. 55, 1224 (1976); B Pire, Nucl. Phys. B114, 11 (1976); P. G. O. Freund and S Nandi, Nuovo Cimento 25A, 395 (1976); V. Matveev, in *Proceedings of the XVIII International Conference on High Energy Physics, Tbilisi, 1976*, edited by N. N. Bogolubov *et al.* (JINR, Dubna, U.S.S.R., 1977).

[18]A. Eide *et al.*, Nucl. Phys. B60, 173 (1973). See also H. I. Miettinen, SLAC Report No. SLAC-PUB-1813, presented at the Third European Symposium on Antinucleon-Nucleon Reactions, Stockholm, 1976 (unpublished).

[19]J. L. Stone *et al.*, Phys. Rev. Lett. 38, 1315 (1977); 38, 1317 (1977).

[20]V. Chabaud *et al.*, Phys. Lett. 41B, 209 (1972).

[21]A. Donnachie and P. R. Thomas, Nuovo Cimento 19A, 279 (1974).

[22]G. G. Hansen, in Proceedings of the VII International Colloquium on Multiparticle Production, Tutzing, 1976 (unpublished).

[23]J. Ellis, M. K. Gaillard, and A. C. Ross, Nucl. Phys. B111, 253 (1976).

[24]Predictions for rising γ/π ratios were given in S. Brodsky, *High Energy Collisions*—1973, edited by C. Quigg (AIP, New York, 1973); G. R. Farrar and S. Frautschi, Phys. Rev. Lett. 36, 1017 (1976); G. R. Farrar, Phys. Lett. 67B, 337 (1977). A complete discussion of QCD and CIM contributions is given by R. Rückl, S. Brodsky, and J. Gunion, Phys. Rev. D (to be published).

[24a]M. Duong-van, K. V. Vasavada, and R. Blankenbecler, Phys. Rev. D 16, 1389 (1977); M. Duong-van and R. Blankenbecler, *ibid.* 17, 1826 (1978).

[25]J. D. Bjorken and J. Kogut, Phys. Rev. D 8, 1371 (1974).

[26]Some of the observed scale breaking can be attributed to simple parton effects that produce power-law breaking. See I. A. Schmidt and R. Blankenbecler, SLAC Reports Nos. SLAC-PUB-1938 and 2010, 1977 (unpublished); Phys. Rev. D 16, 1318 (1977).

[27]As emphasized by the authors of Ref. 8, the jet cross section in QCD could be increased by more than an order of magnitude if gluon-gluon and gluon-quark scattering terms are included. [Note that the quark coupling strength "e_g" is effectively $\frac{3}{2}$ the quark coupling strength "e_q" in SU(3) color, e.g., $d\sigma/dt(gg \to gg) = (81/16)d\sigma/dt(qq \to qq)$ for $s \gg t$.] The estimates for gluon contributions are based on the assumption that the structure function for gluons in the proton $G_{g/p}(x)$ should be normalized to $\sim \frac{1}{2}$ the proton momentum. This may be an overestimate since gluon emission by a color singlet is suppressed, at least at low x. In the color radiation model of S. Brodsky and J. Gunion, Phys. Rev. Lett. 37, 402 (1976), the large amount of gluon emission in deep-inelastic scattering is due to the dynamical separation of quark charges at large $s = (q+p)^2$, rather than the intrinsic presence of gluons in the proton wave function. A detailed discussion is given in D. Jones and J. F. Gunion, SLAC report (in preparation).

[28]W. Furmanski and J. Wosiek, Acta Phys. Polonica B8, 633 (1977). R. Baier, J. Cleymans, K. Kinoshita, and B. Petersson, Nucl. Phys. B118, 139 (1977). R. Baier and B. Petersson, in *Leptons and Multileptons*, proceedings of the XII Recontre de Moriond, Flaine, France, edited by J. Trân Thanh Vân (Editions Frantières, Paris, 1977); J. Ranft, *ibid*; G. Randt and J. Ranft, *ibid.*

[29]For a recent discussion of charge retention in quark and multiquark jets and applications, see S. J. Brodsky and N. Weiss, Phys. Rev. D 16, 2325 (1977); T. DeGrand and H.I. Miettinen, SLAC report (unpublished).

[30]E. Malamud, in Proceedings of the VIII International Symposium on Multiparticle Dynamics, Kaysersberg, 1977 (unpublished); C. Bromberg *et al.*, Phys. Rev. Lett. 38, 1447 (1977); Cormell *et al.*, Fermilab Report No. 77-89 (10-3-77) (unpublished).

[31]The overshoot in F_{eff} is due in part to the particular form (3.1) chosen for the structure functions. Smoother structure functions can give $F_{\text{eff}}(x_T)$ which rise smoothly to their asymptotic value as $x_T \to 1$.

[32]The extra iteration accounts in part for the differences between our approach and that of B. Pire, Phys. Rev. D 15, 3475 (1977), who was one of the first to consider the normalizations of large-transverse-momentum subprocesses.

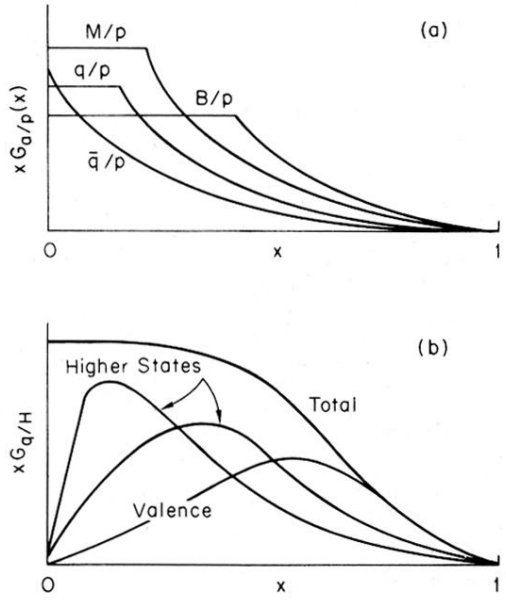

FIG. 1. (a) A schematic of the simplified structure functions used to estimate rates in the text. (b) The manner in which the higher Fock states enter to produce the total structure function.

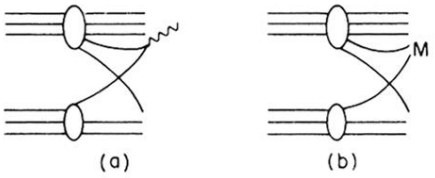

FIG. 10. Illustrating the simple and direct relation between (a) photon and (b) meson production for one type of basic process.

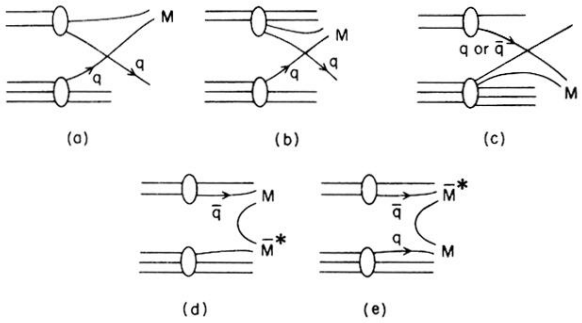

FIG. 11. The five important contributions to meson production by meson beams. The direct process is (a), and the quark-meson process in which the intermediate meson arises from the (b) incident meson and (c) proton target are also shown. The two possible fusion processes are shown in (d) and (e).

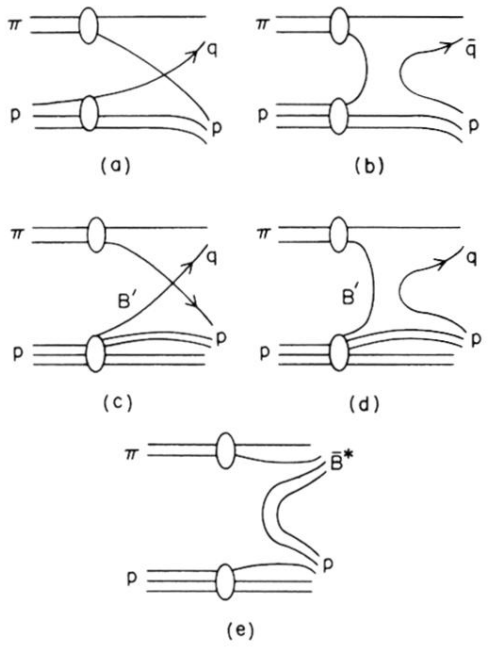

FIG. 12. The five dominant contributions to baryon (and antibaryon) production by meson beams.

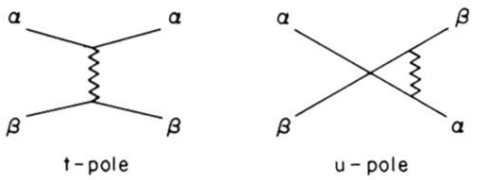

FIG. 13. Lowest-order diagrams for quark-quark scattering via gluon exchange.

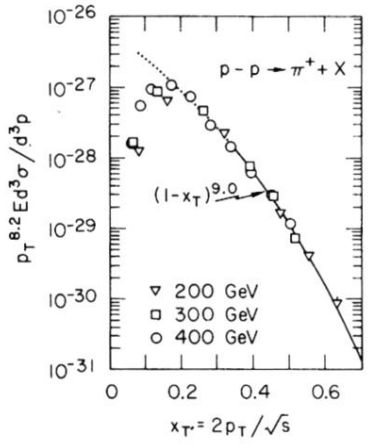

FIG. 14. Scaling-law fit to the cross section $pp \rightarrow \pi^+ X$, $\theta_{c.m.} \cong 90°$, $x_T = 2p_T/\sqrt{s} > 0.3$. From Ref. 1.

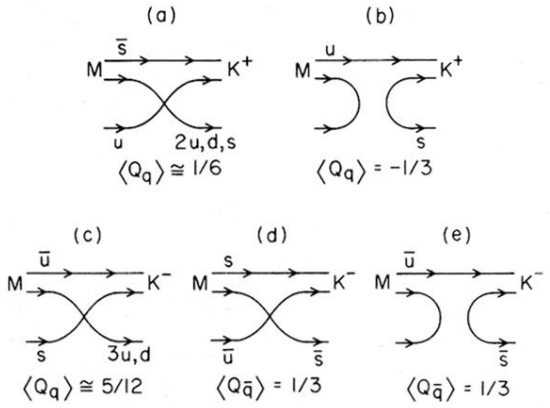

FIG. 15. Dominant CIM diagrams for $Mq \to K^{\pm} q'$ illustrating the final-state charge correlations.

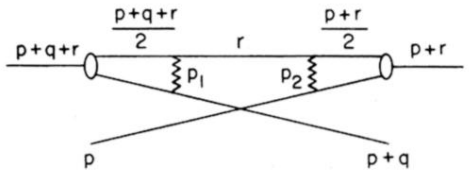

FIG. 16. Diagram for quark-meson scattering using the iteration of the gluon-exchange kernel in both Bethe-Salpeter wave functions.

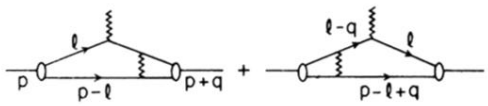

FIG. 17. Diagrams for meson form factor at large momentum transfer in which only one wave function is iterated.

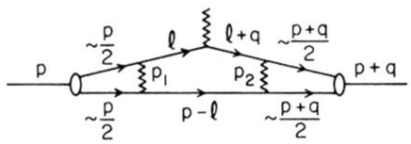

FIG. 18. Diagram for meson form factor using the iternation of the gluon exchange kernel in both Bethe-Salpeter kernels.

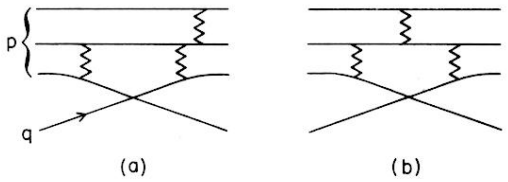

FIG. 2. Two examples of graphs that contribute to quark-proton scattering.

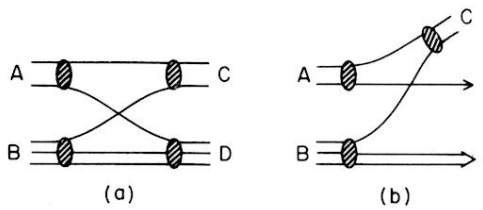

FIG. 3. (a) Typical exclusive scattering contribution to $MB \to MB$ arising from constituent interchange. (b) The corresponding inclusive direct process for $MB \to MX$ illustrating the simple connection to the structure function.

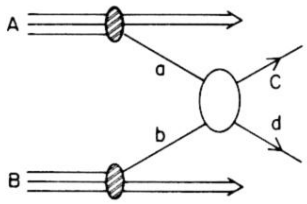

FIG. 4. The double-bremsstrahlung contribution to the prompt inclusive rate for $A + B \rightarrow C + X$. The hard-scattering contribution for the cross section is given in Eq. (1).

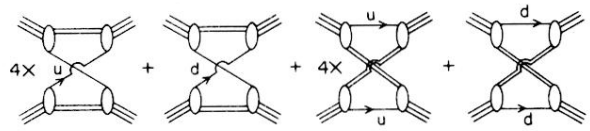

FIG. 5. The various coherent contributions to elastic proton-proton scattering and their respective weightings.

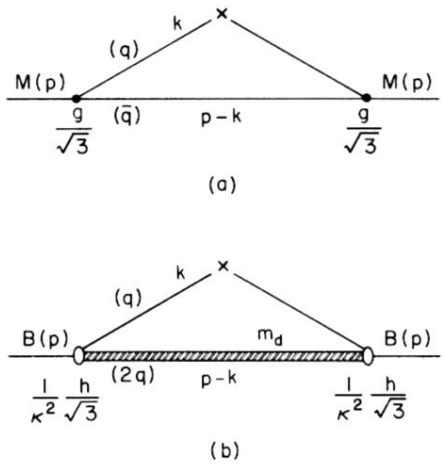

FIG. 6. The momentum routings and the couplings constants used to compute the valence contributions to the (a) meson and (b) baryon structure functions and sum rules.

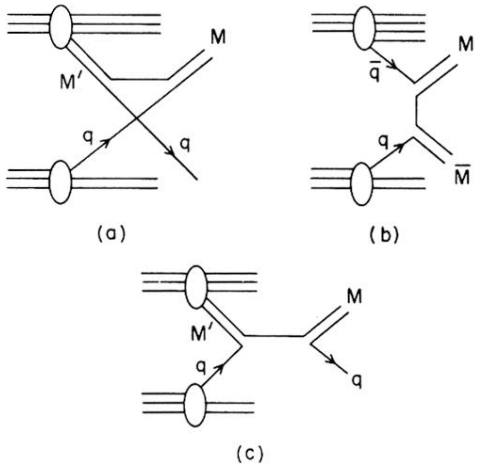

FIG. 7. Various contributions to $p\bar{p} \to MX$ reactions. (a) The (ut) graph for the $qM \to qM$ basic process. (b) The corresponding inclusive direct process for $MB \to MX$ illustrating the simple connection to the structure function.

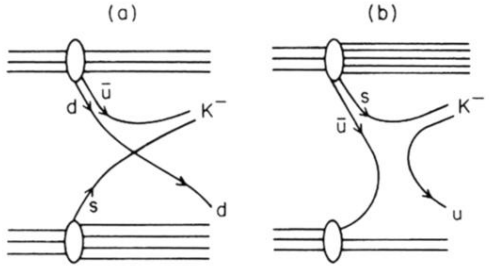

FIG. 8. The two dominant contributions to the ϵ^{13} term in the $pp \to K^- X$ yield; (a) the strangeness arising from the target and (b) the beam.

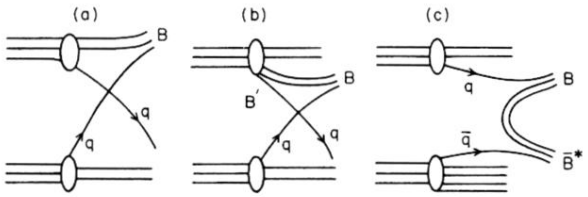

FIG. 9. Baryon production from proton beams; (a) the direct-scattering graph, (b) beam bremsstrahlung (of a mesonic spectator system), and (c) the fusion process, are shown.